1

Introduction to Shape Memory Alloys

P. K. Kumar and D. C. Lagoudas

Shape Memory Alloys (SMAs) have been on the forefront of research for the last several decades. They have been used for a wide variety of applications in various fields. This chapter introduces the unique behavior that is observed in SMAs. Their characteristic properties and associated microstructural behavior will be discussed in detail. The different types of SMAs and some common applications will also be reviewed.

1.1 Introduction: Overview of Active Materials

For centuries, metals have played an important role as structural materials. Techniques of alloying, smelting, and forging have been evolving since the bronze and iron ages. With advancements in science and technology, and a deeper understanding of the effects of microstructure and processing techniques on the material behavior, the field of material science has radically improved through the past decades. The capability to engineer different material properties (mechanical, thermal, electrical, etc.) for a variety of applications has enabled the development of new alloys and composites. The demand for lighter, stronger materials with tailored properties that address both stringent structural requirements and provide additional engineering functionality (e.g., sensing, actuation, electromagnetic shielding) has spawned a new branch of materials called *multifunctional materials*. A specialized subgroup of multifunctional materials exhibiting sensing and actuation capabilities is known as *active materials*.

In sensing, a mechanical signal is converted into a non-mechanical output (e.g., voltage), while an actuator converts a non-mechanical input (e.g., electrical power) into a mechanical output. Active materials in general exhibit a mechanical response when subjected to a non-mechanical field (thermal, electrical, magnetic, optical, etc.). The mechanical response of these materials is typically one or more orders of magnitude greater than the response resulting from conventional material behavior such as thermal expansion. Some examples of active materials include piezoelectrics and electrostrictives (coupling of mechanical with electric fields), piezomagnetics and magnetostrictives (coupling of mechanical with magnetic fields), and shape memory materials

D.C. Lagoudas (ed.), *Shape Memory Alloys*, DOI: 10.1007/978-0-387-47685-8_1,

(coupling of thermal with mechanical fields). Active materials can be further subdivided into materials that exhibit direct or indirect coupling. Piezoceramics, piezoelectric polymers, magnetostrictive ceramics, shape memory alloys and magnetic shape memory alloys are examples of active materials that exhibit a direct coupling. This implies that either the mechanical or the non-mechanical field can serve as an input while the other as the output. In contrast, for active materials such as electro-rheological fluids (ERF) and magneto-rheological fluids (MRF), a change in the electric field or the magnetic field can indirectly couple with the mechanical behavior through a change in the viscosity of the fluid. This indirect, or one-way, coupling usually lacks the reciprocity of the two-way coupling exhibited by active materials that directly couple two fields.

The suitability of an active material with direct coupling for actuation applications depends on many factors. Two key design drivers are the actuation energy density (available work output per unit volume) and the actuation frequency of the material. An ideal active material would have both a high actuation energy density and a high actuation frequency. Figures 1.1 and 1.2 compare the actuation energy densities and the actuation frequencies, respectively, of some common active materials. The actuation energy density is denoted in Fig. 1.1 by the dotted lines and is defined as the product of the actuation strain (related to the stroke of an actuator) with the actuation stress, assuming here that the active material is operating under constant stress. The specific actuation energy density (work output per unit mass)

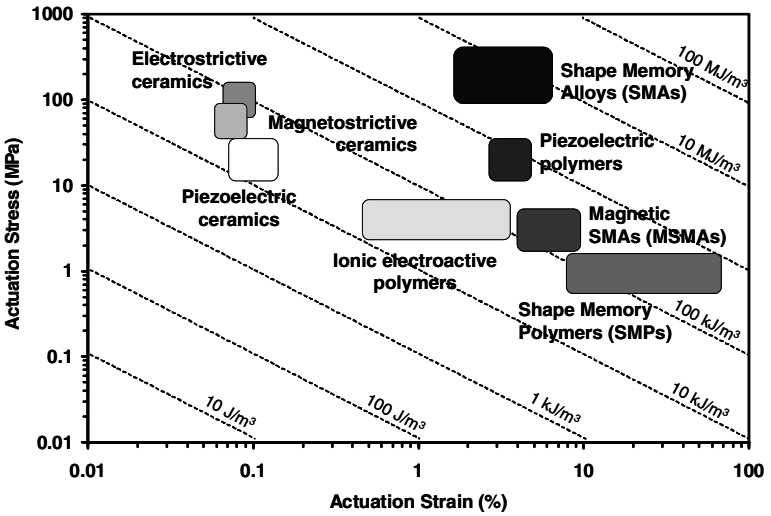

Fig. 1.1. Actuation energy density diagram indicating typical ranges of actuation stress, actuation strain, and the actuation energy densities of different active materials that exhibit direct coupling.

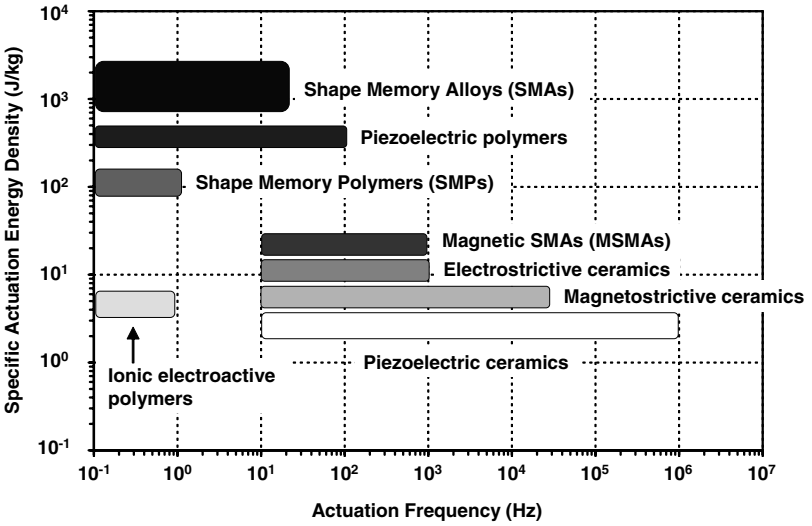

Fig. 1.2. Actuation frequency diagram comparing the actuation frequency ranges of different active materials that exhibit direct coupling.

for a specific active material can be calculated from Fig. 1.1 by dividing the actuation energy density by the mass density.

Shape Memory Alloys (SMAs) are a unique class of shape memory materials with the ability to recover their shape when the temperature is increased. An increase in temperature can result in shape recovery even under high applied loads therefore resulting in high actuation energy densities as shown in Fig. 1.1. In addition, under specific conditions, SMAs can absorb and dissipate mechanical energy by undergoing a reversible hysteretic shape change when subjected to applied mechanical cyclic loading. These unique characteristics of SMAs have made them popular for sensing and actuation, impact absorption and vibration damping applications. SMAs do, however, exhibit low frequency response, as shown in Fig. 1.2. Higher actuation frequencies are achievable for a class of SMAs called magnetic shape memory alloys, which have recently been investigated.

The application of SMAs spans a wide variety of industrial sectors such as aerospace, automotive, biomedical, and oil exploration. Over the past few decades, several key works have explored the microstructural mechanisms, engineering effects, and applications of shape memory alloys, including the experimental work of Jackson and coworkers [1], the application considerations of Duerig and others [2], and the comprehensive summaries of Perkins, Funakubo, and Otsuka and Wayman [3–5]. In the context of the current textbook, this chapter will provide insights into the history of SMAs, their properties, their microstructural behavior, and their varied industrial applications.

1.2 Shape Memory Alloys - A Brief History

The discovery of martensite in steels in the 1890s by Adolf Martens was a major step toward the eventual discovery of shape memory alloys. The martensitic transformation was perhaps the most widely studied metallurgical phenomenon during the early 1900s. The martensitic transformation, as observed in the Fe-C system, was established as an irreversible process. The concept of thermoelastic martensitic transformation, which explained the reversible transformation of martensite, was introduced in 1949 by Kurdjumov and Khandros [6], based on experimental observations of the thermally reversible martensitic structure in CuZn and CuAl alloys. By 1953, the occurance of thermoelastic martensitic transformation was demonstrated in other alloys such as InTl and CuZn.

The reversible martensitic transformation and the alloys that exhibited them remained unutilized until 1963. The breakthrough for engineering applications occurred with the discovery of NiTi by Buehler and coworkers while investigating materials useful for heat shielding [7]. It was noticed that in addition to its good mechanical properties, comparable to some common engineering metals, the material also possessed a shape recovery capability. Following this observation, the term "NiTiNOL" was coined for this NiTi material in honor of its discovery at the Naval Ordnance Laboratory (NOL). The term Shape Memory Effect (SME) was given to the associated shape recovery behavior. The discovery of Nitinol spearheaded active research interest into SMAs. The effects of heat treatment, composition and microstructure were widely investigated and began to be understood during this period [1].

In 1965, studies [8] showed that the addition of a third alloying element such as Co or Fe to the existing NiTi system caused a dramatic decrease in the SMA transformation temperatures. The new alloys inspired the first commercial SMA application, known as Cryofit, where SMA material was used for pipe couplings in F-14 fighter aircraft [9, 10]. The transformation temperatures for Cryofit were so low that, to prevent actuation from occurring before the assembly, the pipe couplings were transported in liquid nitrogen. Continued research to address this issue led to the development of the NiTiNb system in 1989, which was easier to handle due to its larger temperature hysteresis, and found widespread applications in battle damage repairs and in repairs for nuclear reactors [11]. *High Temperature SMAs* (HTSMAs), such as TiPd, TiPt and TiAu (with transformation temperatures greater than 100 °C), were also developed as early as 1970 [12]. Meanwhile, Melton and Mercier [13], while studying the fatigue properties of NiTi in 1978, showed that alloying the material with Cu did not change the transformation temperatures considerably, but narrowed the stress hysteresis. Later in 1999, Miyazaki showed improved fatigue life for NiTiCu alloys [14]. The improved fatigue life and the low cost associated with this material system made it suitable for a wide variety of engineering applications.

Since the initial discovery of Nitinol in 1963, many commercial applications have been developed. During the 1970s, several uses of NiTi in biomedical applications appeared, but it wasn't until the 1990s that NiTi stents made their commercial breakthrough. By this time, SMAs had found additional applications in air conditioning vents, electronic cable connectors, valves and a variety of other products. In addition, over the last decade the demand for actuation under high temperature operating conditions, driven by the aerospace and oil industries, has revived a great deal of interest in the development of HTSMAs. Finally, alloys that exhibit shape change characteristics similar to SMAs but under the influence of a magnetic field have recently been under investigation [15, 16]. The high actuation frequencies and the large strains generated in *Magnetic SMAs* (MSMAs) have made these materials a strong candidate for high frequency actuation devices.

1.3 Phenomenology of Phase Transformation in Shape Memory Alloys

A metallurgical phase diagram for a metallic alloy is a schematic representation of the equilibrium conditions between distinct phases. Phase diagrams consist of equilibrium lines or phase boundaries that separate different phases from each other. For an alloy consisting of at least two elements, the concentration becomes an important variable and is generally represented along the abscissa axis. The other variable commonly used is the temperature, represented along the ordinate axis. A phase diagram can have different control variables (stress, temperature, concentration, electric field etc.) within the bounds of which the equilibrium phases can be represented. For an alloy at a fixed composition (i.e. any vertical line parallel to the ordinate axis), the formation and disassociation of phases with the change in temperature is shown. Similarly, within the typical operating temperature range, SMAs have two phases, each with a different crystal structure and therefore different properties. One is the high temperature phase called *austenite* (A) and the other is the low temperature phase called *martensite* (M). Austenite (generally cubic) has a different crystal structure from martensite (tetragonal, orthorhombic or monoclinic). The transformation from one structure to the other does not occur by diffusion of atoms, but rather by shear lattice distortion. Such a transformation is known as martensitic transformation. Each martensitic crystal formed can have a different orientation direction, called a *variant*. The assembly of martensitic variants can exist in two forms: *twinned* martensite (M^t), which is formed by a combination of "self-accommodated" martensitic variants, and *detwinned* or reoriented martensite in which a specific variant is dominant (M^d). The reversible phase transformation from austenite (parent phase) to martensite (product phase) and vice versa forms the basis for the unique behavior of SMAs.

Upon cooling in the absence of an applied load, the crystal structure changes from austenite to martensite. The phase transition from austenite to martensite is termed the *forward transformation*. The transformation results in the formation of several martensitic variants, up to 24 for NiTi. The arrangement of variants occurs such that the average macroscopic shape change is negligible, resulting in *twinned martensite*. When the material is heated from the martensitic phase, the crystal structure transforms back to austenite, and this transition is called *reverse transformation*, during which there is no associated shape change.

A schematic of the crystal structures of twinned martensite and austenite for an SMA and the transformation between them is shown in Fig. 1.3. There are four characteristic temperatures associated with the phase transformation. During the forward transformation, austenite, under zero load, begins to transform to twinned martensite at the *martensitic start temperature* (M_s) and completes transformation to martensite at the *martensitic finish temperature* (M_f). At this stage, the transformation is complete and the material is fully in the twinned martensitic phase. Similarly, during heating, the reverse transformation initiates at the *austenitic start temperature* (A_s) and the transformation is completed at the *austenitic finish temperature* (A_f).

If a mechanical load is applied to the material in the twinned martensitic phase (at low temperature), it is possible to detwin the martensite by reorienting a certain number of variants (see Fig. 1.4). The detwinning process results in a macroscopic shape change, where the deformed configuration is retained when the load is released. A subsequent heating of the SMA to

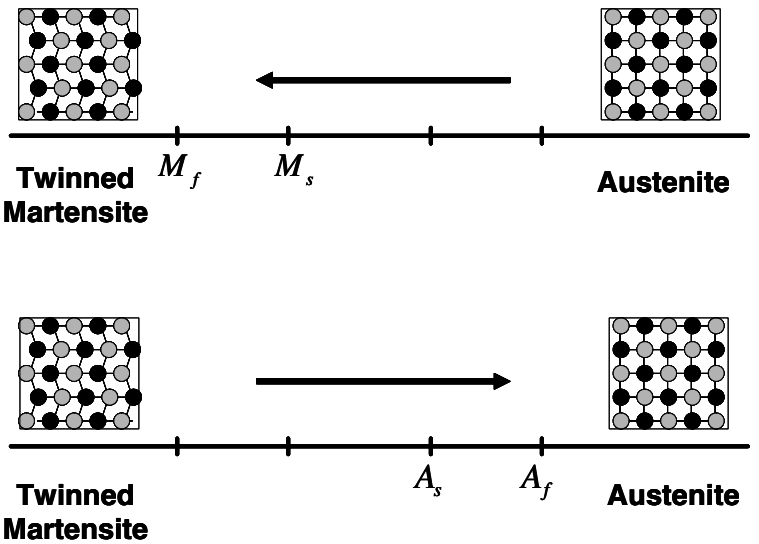

Fig. 1.3. Temperature-induced phase transformation of an SMA without mechanical loading.

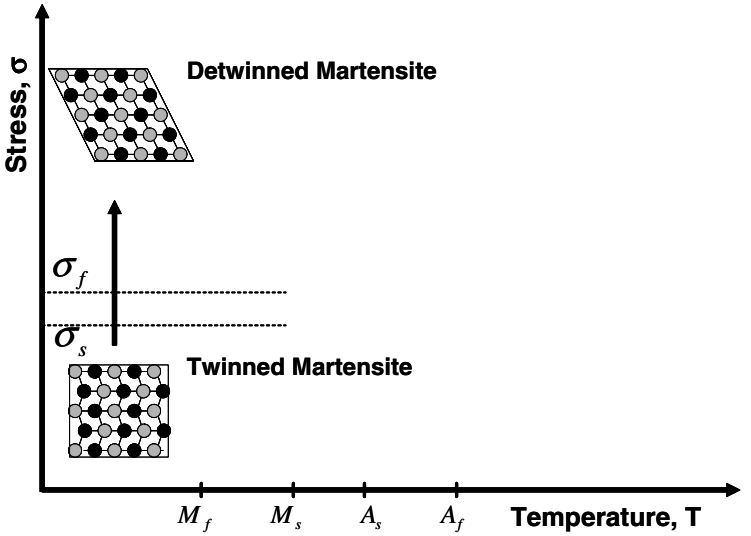

Fig. 1.4. Schematic of the shape memory effect of an SMA showing the detwinning of the material with an applied stress.

a temperature above A_f will result in a reverse phase transformation (from detwinned martensite to austenite) and will lead to complete shape recovery (see Fig. 1.5). Cooling back to a temperature below M_f (forward transformation) leads to the formation of twinned martensite again with no associated

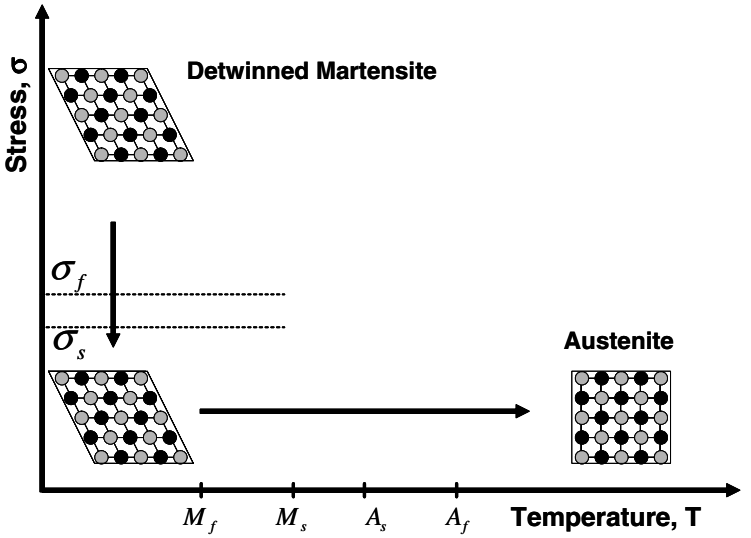

Fig. 1.5. Schematic of the shape memory effect of an SMA showing the unloading and subsequent heating to austenite under no load condition.

shape change observed. The process described above is referred to as the *Shape Memory Effect* (SME). The load applied must be sufficiently large to start the detwinning process. The minimum stress required for detwinning initiation is termed the *detwinning start stress* (σ_s). Sufficiently high load levels will result in complete detwinning of martensite where the corresponding stress level is called the *detwinning finish stress* (σ_f).

When the material is cooled with a mechanical load greater than σ_s applied in the austenitic phase, the phase transformation will result in the direct formation of detwinned martensite, producing a shape change. Reheating the material will result in shape recovery while the load is still applied. A schematic of the above-described loading path is shown in Fig. 1.6. Recognizing that the forward and reverse transformations occur over a range of temperatures (M_s to M_f, A_s to A_f) for a given SMA composition, we can construct transformation regions in the stress-temperature space. The transformation temperatures strongly depend on the magnitude of the applied load, with higher values of applied load leading to higher transformation temperatures. As a consequence, the transformation regions representing the A$\rightarrow M^d$ and $M^d\rightarrow$A transformations have a positive slope in stress-temperature space. Irrespective of the nature of applied load (tension or compression), the transformation temperatures increase with an increase in the magnitude of the load. Under an applied uniaxial tensile load with a corresponding stress, σ, the new transformation temperatures are represented as M_f^σ, M_s^σ, A_s^σ and A_f^σ for martensitic finish, martensitic start, austenitic start and the austenitic finish temperatures, respectively. It should be noted that σ refers to the magnitude

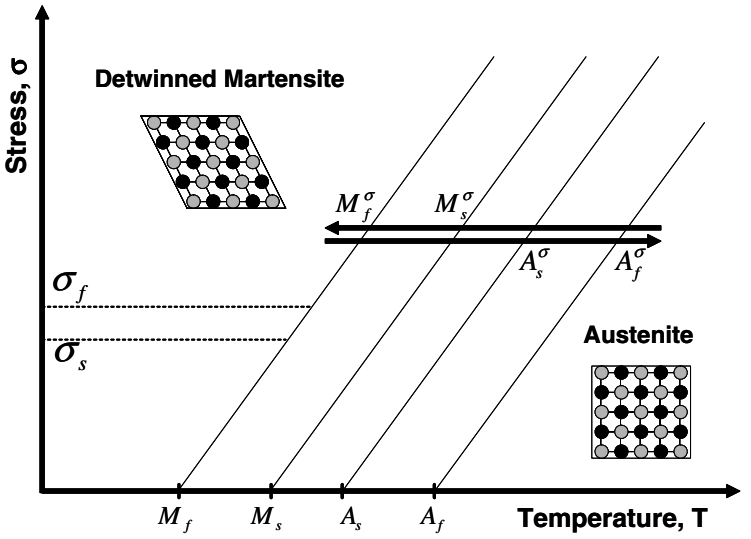

Fig. 1.6. Temperature-induced phase transformation in the presence of applied load.

of a uniaxial stress state or an appropriate scalar measure for a multiaxial stress state, as will be explained in Chapter 3.

In addition to thermally induced phase transformation, transformation can also be induced by applying a sufficiently high mechanical load to the material in the austenitic phase. The result of this load is fully detwinned martensite created from austenite. If the temperature of the material is above A_f, a complete shape recovery is observed upon unloading to austenite. This material behavior is called the *pseudoelastic effect*. A loading path demonstrating the pseudoelastic effect is shown schematically in Fig. 1.7, while the associated macroscopic shape change due to the applied load is captured in the resulting stress-strain diagram, as shown schematically in Fig. 1.8. The stress levels at which the martensite transformation initiates and completes are denoted by σ^{Ms} and σ^{Mf}, respectively. Similarly, as the SMA is unloaded, the stress levels at which the material initiates and completes its reverse transformation to austenite are denoted by σ^{As} and σ^{Af}, respectively. If the material in the austenitic phase is tested above the M_s temperature, but below the A_f temperature, only partial shape recovery is observed.

Figure 1.9 shows a schematic representation of the different phases of the SMA, which include the austenitic phase and both the twinned (self-accommodated) and detwinned martensite, along with the transition zones, in a stress-temperature diagram. Such a diagram, illustrating the different phases in a stress-temperature space for a given SMA with fixed composition, is called the *phase diagram*. Note that the phase diagram of Fig. 1.9 is a special case of the metallurgical phase diagram introduced in the beginning of Section 1.3, which involves composition as another variable. Construction of the

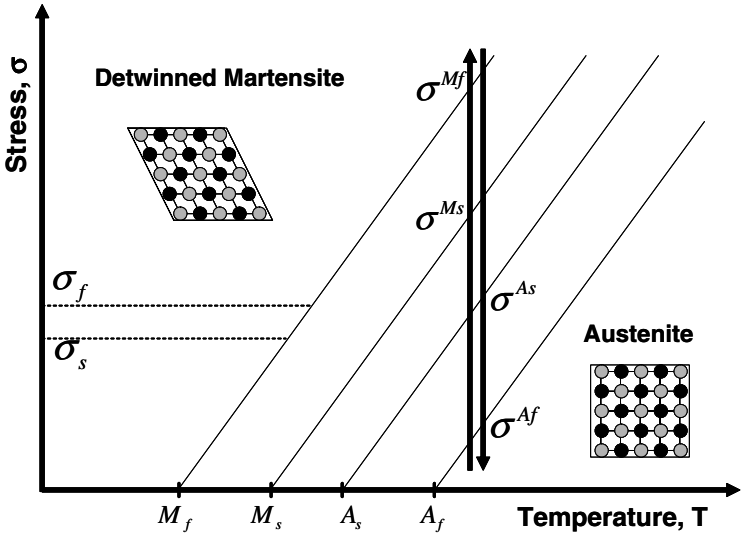

Fig. 1.7. A pseudoelastic loading path.

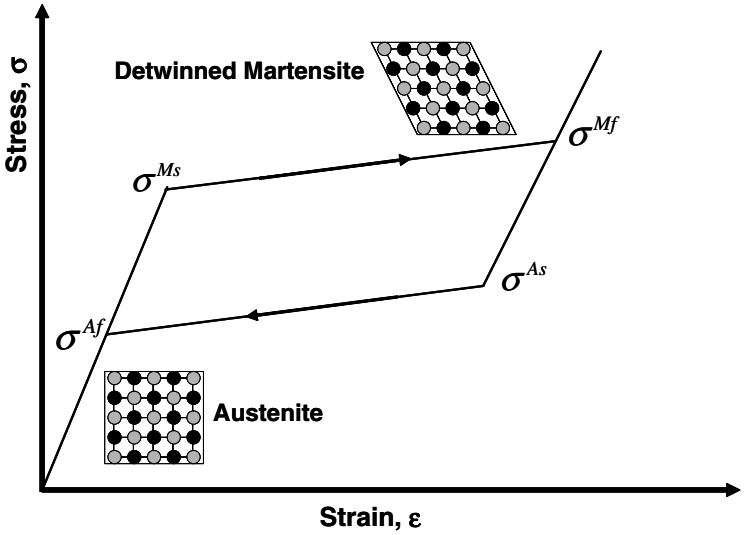

Fig. 1.8. Schematic of a pseudoelastic stress-strain diagram.

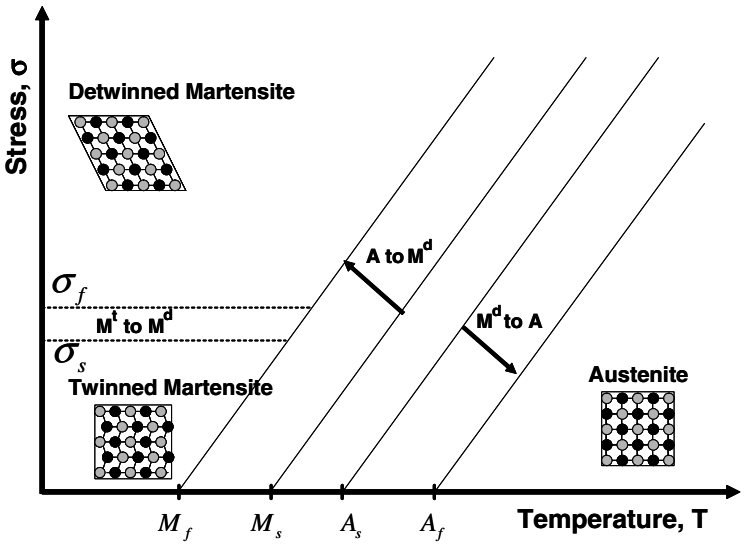

Fig. 1.9. Schematic of a stress-temperature phase diagram for an SMA.

phase diagram involves the interpretation of the SMA material response subjected to various thermomechanical loading paths resulting in shape memory thermal actuation under load and pseudoelastic behavior. In the following sections, the two important characteristics of SMAs, namely the shape memory effect and pseudoelasticity, will be discussed in more detail.

1.4 Shape Memory Effect

An SMA exhibits the *shape memory effect* (SME) when it is deformed while in the twinned martensitic phase and then unloaded while at a temperature below A_s. When it is subsequently heated above A_f, the SMA will regain its original shape by transforming back into the parent austenitic phase. The nature of the SME can be better understood by following the thermomechanical loading path in a combined stress-strain-temperature space as shown in Fig. 1.10. Figure 1.10 represents experimental data for a typical NiTi specimen tested under uniaxial loading. The stress σ is the uniaxial stress on the specimen due to an applied load. The corresponding strain ε is the change in the length of the specimen along the direction of applied load, normalized by the original length.

Starting from the parent phase (point A in Fig. 1.10), the stress-free cooling of austenite below the forward transformation temperatures (M_s and M_f) results in the formation of twinned martensite (point B). When the twinned martensite is subjected to an applied stress that exceeds the start stress level (σ_s), the reorientation process is initiated, resulting in the growth of certain favorably oriented martensitic variants that grow at the expense of other less favorable variants. The stress level for reorientation of the variants is far lower than the permanent plastic yield stress of martensite. The detwinning process is completed at a stress level, σ_f, that is characterized by the end of

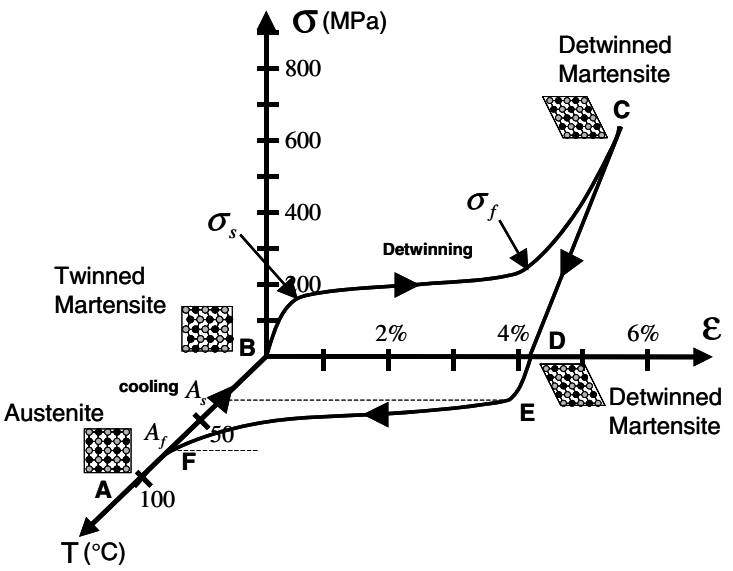

Fig. 1.10. Stress-strain-temperature data exhibiting the shape memory effect for a typical NiTi SMA.

the plateau in the σ-ε diagram in Fig. 1.10. The material is then elastically unloaded from C to D and the detwinned martensitic state is retained. Upon heating in the absence of stress, the reverse transformation initiates as the temperature reaches A_s, (at E) and is completed at temperature A_f (point F), above which only the parent austenitic phase exists. In the absence of permanent plastic strain generated during detwinning, the original shape of the SMA is regained (indicated by A). The strain recovered due to the phase transformation from detwinned martensite to austenite is termed as the transformation strain (ε^t). Subsequent cooling to martensite will again result in the formation of self-accommodated twinned martensitic variants with no associated shape change, and the whole cycle of the SME can be repeated. The above described phenomenon is called *one-way shape memory effect*, or simply SME, because the shape recovery is achieved only during heating after the material has been detwinned by an applied mechanical load.

Example 1.1. In order to review the SME, let us consider an SMA wire whose behavioral characteristics are represented by the stress-strain-temperature diagram shown in Fig. 1.10. The SME of the wire is used for a one time actuation application. The wire, held at a temperature below the M_f (twinned martensitic state), is stretched along the axial direction. Under the applied loading, the material exhibits an elastic behavior and continues to elastically deform as the stress is increased. When the stress due to the applied loading reaches approximately 150MPa, the SMA wire begins to elongate significantly with a small increment in the stress level. This point marks the beginning of the martensitic detwinning in the wire. The detwinning continues until the total strain reaches approximately 4% and the entire wire has detwinned. At this point, the wire begins to stiffen again as the stress is increased. The end of the detwinning process is marked by the change in the slope during loading. The detwinned wire elastically unloads as the stress is released and the strain induced due to the detwinning is not recovered. This detwinned wire is then attached on the structure for the actuation application. During the actuation process, the wire is heated using a thermal source such as resistive heating. As the temperature of the wire increases, the wire initially undergoes thermal expansion. However, as the temperature reaches the austenitic start temperature of approximately 30 °C, the detwinned martensite in the material begins transformation into austenite. This results in the contraction (i.e., actuation) of the SMA. As the temperature reaches a value above 70 °C, the transformation (actuation) is complete and the wire is in the austenitic state. The exact austenitic finish temperature will depend on the stress of the SMA wire during the reverse transformation. Subsequent cooling returns the wire to the twinned state in the absence of a recovery stress applied by the structure on which the SMA is attached. The wire would then have to be detwinned for the next actuation cycle unless the structure can provide sufficient stress for detwinning upon cooling.

1.5 Pseudoelasticity

The *pseudoelastic* behavior of SMAs is associated with stress-induced transformation, which leads to strain generation during loading and subsequent strain recovery upon unloading at temperatures above A_f. A pseudoelastic thermomechanical loading path generally starts at a sufficiently high temperature where stable austenite exists, then develops under an applied load to a state at which detwinned martensite is stable, and finally returns to the austenitic phase when returned to zero stress state. An example of this path ($a \rightarrow b \rightarrow c \rightarrow d \rightarrow e \rightarrow a$) is shown in Fig. 1.11 as path 1. Most commonly, a pseudoelastic test is performed at a nominally constant temperature above A_f. The loading path for such a test is shown as path 2 in Fig. 1.11.

To illustrate the pseudoelastic behavior in greater detail, let us consider the thermomechanical loading path ($\mathsf{A} \rightarrow \mathsf{B} \rightarrow \mathsf{C} \rightarrow \mathsf{D} \rightarrow \mathsf{E} \rightarrow \mathsf{F} \rightarrow \mathsf{A}$) in Fig. 1.11, which starts at zero stress at a temperature above A_f. The corresponding σ-ε experimental data for the loading path is shown in Fig. 1.12. When a mechanical load is applied, the parent phase (austenite) undergoes elastic loading ($\mathsf{A} \rightarrow \mathsf{B}$). At a specific load level, the loading path intersects the surface for initiation of martensitic transformation on the phase diagram. This marks the stress level (σ^{Ms}) for the onset of transformation into martensite. Note that the stress-induced transformation from austenite to martensite is accompanied by the generation of large inelastic strains as shown in the stress-strain diagram of Fig. 1.12. The transformation proceeds ($\mathsf{B} \rightarrow \mathsf{C}$), to the stress level ($\sigma^{Mf}$) where the loading path intersects the M_f transformation surface, indicating the end of the transformation.

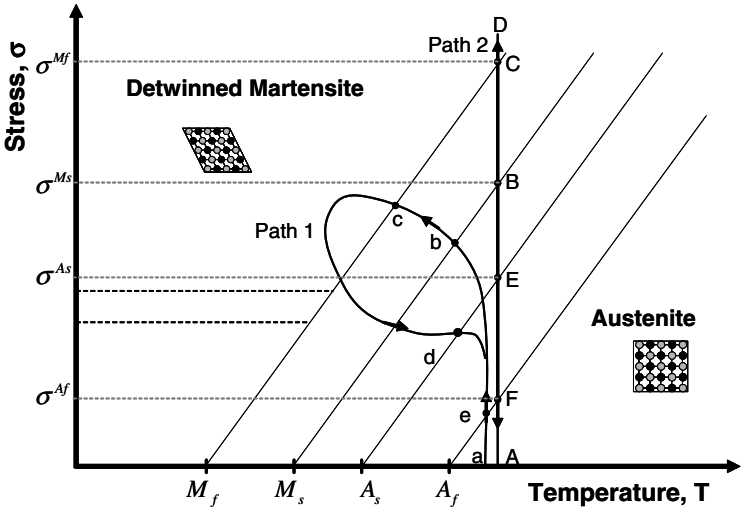

Fig. 1.11. Phase diagram and two possible pseudoelastic loading paths.

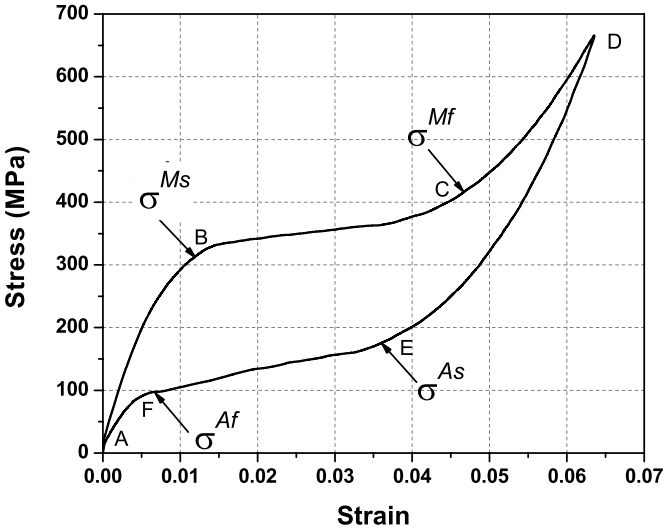

Fig. 1.12. A typical SMA pseudoelastic loading cycle.

The completion of martensitic transformation is indicated by a distinct change in slope on the σ-ε curve, which is associated with the elastic loading of the martensitic phase. A subsequent increase in the stress causes no further transformation and only the elastic deformation of detwinned martensite occurs (C $\rightarrow$ D). When the stress is released gradually by unloading, the martensite elastically unloads along the path (D $\rightarrow$ E). At point E, the unloading path intersects the austenitic start surface (at σ^{As}), which causes the martensite to revert to austenite. The process is accompanied by the recovery of the strain due to phase transformation at the end of unloading. The end of the transformation back into austenite is denoted by the point at which the σ-ε unloading curve rejoins the elastic region of austenite (point F corresponding to stress σ^{Af}). The material then elastically unloads to A. The forward and reverse phase transformation during a complete pseudoelastic cycle results in a hysteresis, which, in the σ-ε space, represents the energy dissipated in the transformation cycle. The transformation stress levels and the size of the hysteresis vary depending on the SMA material and testing conditions.

The detwinned martensite that forms from austenite as a result of the applied stress during Path 1 or 2 in Fig. 1.11 is one form of *stress-induced martensite* (SIM). SIM, in general, is martensite that forms from austenite in the presence of stress. There are many thermomechanical loading paths that can result in the formation of SIM.

Generally, the term *pseudoelasticity* describes both *superelastic* behavior and so-called *rubber-like* behavior [5]. The reversible phase transformation (described in the previous paragraph) caused by a thermomechanical loading path is strictly called the superelastic behavior. The rubber-like effect is an exclusive behavior of the martensite phase only and occurs due to the reversible reorientation of martensite. In some cases, aging the martensitic phase can enable the reversal of the martensitic detwinning process upon unloading at temperatures below M_f. The resulting σ-ε curve is similar to the superelastic curve, and this phenomenon is called the *rubber-like* effect to emphasize the similarities with the nonlinear elastic behavior of rubber. In SMAs exhibiting the rubber-like effect, the stress required to detwin martensite is very small compared to σ^{Ms}. We will not consider the rubber-like effect any further, and the term pseudoelasticity will refer to the superelastic behavior of SMAs only.

1.6 Cyclic Behavior of SMAs

We have studied the one-way SME behavior in SMAs. Sometimes an SMA can exhibit repeatable shape changes under no applied mechanical load when subjected to a cyclic thermal load. This behavior is termed *two-way shape memory effect* (TWSME). The TWSME can be observed in a SMA material which has undergone repeated thermomechanical cycling along a specific loading path (*training*). Repetition along a loading path for a large number of cycles can induce changes in the microstructure, which causes macroscopically observable permanent changes in the material behavior.

Training an SMA refers to a process of repeatedly loading the material following a cyclic thermomechanical loading path until the hysteretic response of the material stabilizes and the inelastic strain saturates. Let us consider the case of cyclic thermal loading of an SMA specimen under a constant applied stress (Fig. 1.13). During the first thermal cycle, only a partial recovery of the strain generated during cooling is observed upon heating with some permanent (irrecoverable or plastic) strain generated during the cycle. A small, permanent strain remains after each thermal cycle is completed. The additional permanent strain associated with each consecutive cycle begins to gradually decrease until it practically ceases to further accumulate (Fig. 1.13). A similar behavior can be noticed in the case of mechanically cycling an SMA repeatedly in its pseudoelastic regime, until saturation takes place (Fig. 1.14). The TWSME behavior can also be achieved by adopting different training sequences [17, 18]. A more recent technique that leads to TWSME deals with aging the material under stress in the martensitic state [19].

TWSME is a result of defects introduced during training. These permanent defects create a residual internal stress state, thereby facilitating the formation of preferred martensitic variants when the SMA is cooled in the

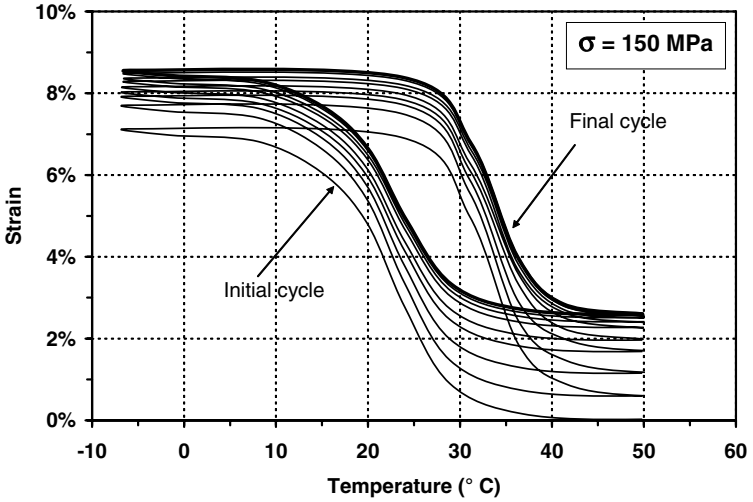

Fig. 1.13. Thermal cyclic loading (50 cycles) of a NiTi shape memory alloy wire under constant load of 150 MPa [18].

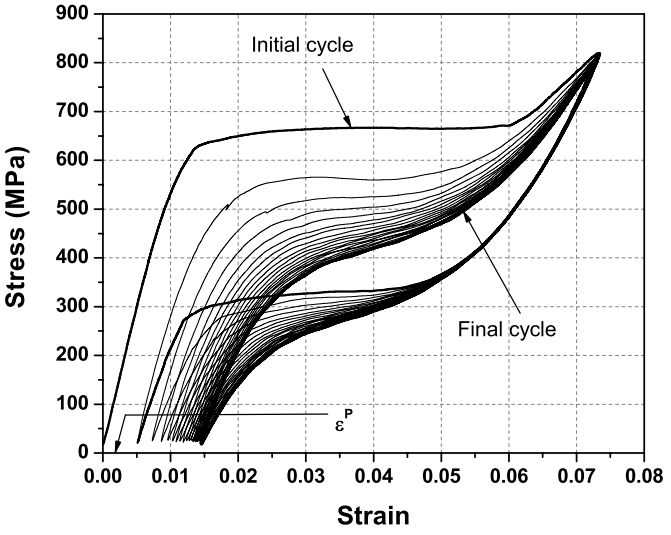

Fig. 1.14. Pseudoelastic response of an as-received NiTi wire with $A_f = 65\,^{\circ}\mathrm{C}$, tested at a temperature of 70 °C. Also shown is the stabilized pseudoelastic hysteresis loop after 20 cycles.

absence of external loads. If the internal stress state is modified for any reason (e.g., aging at high temperature or mechanical overload), the TWSME will be perturbed [20].

1.7 Transformation Induced Fatigue in SMAs

Since SMAs are widely preferred for actuation and sensing applications that require multiple cycles, it is now important to extend what we learned about cyclic effects to the topic of transformation induced fatigue behavior. The fatigue behavior of SMAs depends on the material processing (fabrication process, heat treatment, etc.), the type of loading conditions (applied stress, strain, temperature variations, environment, etc.), and transformation induced microstructural modifications (e.g., defects on grain boundaries due to strain incompatibilities). In most SMA applications, a large number of transformation cycles are induced by repeating a loading path that exhibits either pseudoelasticity or thermally induced phase transformation under applied load. As discussed in the previous section, repeated loading along a thermomechanical path causes gradual microstructural changes. These changes cause the degradation of the SMA behavior leading to low cycle fatigue as opposed to high cycle fatigue most commonly observed in loading paths operating in a purely elastic regime of a material. This section will provide a brief review of mechanically and thermally induced transformation fatigue behavior of SMAs.

Mechanically induced fatigue behavior of SMAs is typically examined by performing rotating bending tests or by mechanically cycling the material on the load frame between two stress or strain levels along a given loading path [18, 21]. Such mechanical cycling can be performed to induce a complete transformation (i.e., cycled between complete austenite and martensite phase) or partial transformation (cycling between states where one or both end limits are not purely martensite or austenite but a mixture). If the deformation or stress level applied to the SMA specimen remains within the elastic regime, this can lead to fatigue life as high as $\sim 10^7$ cycles. However, in some cases, the material can be taken through detwinning or stress induced martensitic transformation by applying sufficiently high load levels. In such cases, the material fails considerably earlier in what is termed "transformation-induced low cycle fatigue," with a fatigue life of the order of thousands of cycles [22, 23].

Similar to mechanically induced transformation fatigue, thermally-induced transformation fatigue behavior of SMAs is extremely important to study for actuation applications. Fatigue life for SMAs undergoing thermally-induced transformation cycles under applied load is dictated by the amount of transformation strain allowed to occur (partial or complete transformation) as well as the stress level under which the material is cycled. The amount of cyclic transformation strain allowed in the material can significantly affect the number of cycles to failure [24]. Under conditions of partial transformation, SMAs

can exhibit much higher fatigue lives. A partial transformation limits the generation of martensite and the associated transformation strain, which causes a significant improvement in the fatigue life of the alloy [25–27].

Typical fatigue test data for complete and partial transformation in a NiTiCu material under a fixed stress level of 200 MPa is shown in Fig. 1.15. In the figures, the line A represents the strain in the SMA wire specimen at the end of each cycle after cooling to a certain level. Similarly, line B represents the strain in the SMA after heating to a certain level. In the complete transformation case, Fig. 1.15a, these levels pertain to complete martensitic transformation. In Fig. 1.15b, lines A and B represent strains generated during partial martensitic transformation. Taking the difference between these strain values at a given cycle and accounting for the effects of elastic moduli, one can obtain the transformation strain for the complete and partial transformations as shown in Fig. 1.15a and Fig. 1.15b respectively. The fatigue life is improved by approximately a factor of seven for a partial transformation and the amount of stable maximum transformation strain is reduced by a factor of three.

Other microstructural characteristics such as precipitate size and crystallographic orientation can also have a significant impact on the fatigue life of SMAs [28]. Heat treating the material under optimal conditions can also improve the fatigue behavior of SMAs. However, high annealing temperatures or chemically active environments can result in oxidation and corrosion, leading to crack nucleation and growth, thus reducing the fatigue life of SMAs [23, 27, 29, 30].

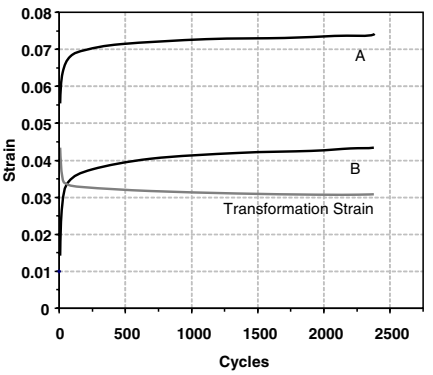

(a) Complete transformation

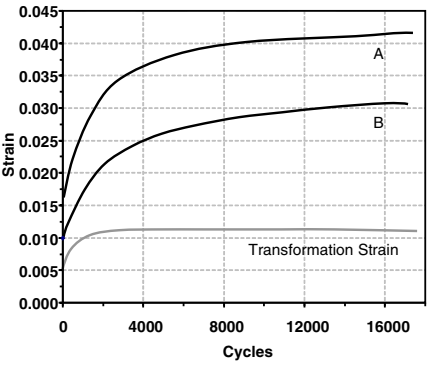

(b) Partial transformation

Fig. 1.15. Thermally-induced transformation fatigue results for 200 MPa applied stress level. Curves indicate strain levels in martensite (A) and complete or partial austenite (B), in addition to recoverable transformation strain.

1.8 Crystallography of Martensitic Transformation

The transformation from austenite to martensite is a diffusionless transformation that occurs by shear distortion of the lattice structure (movement of atoms from their original position). This martensitic transformation possesses well-defined characteristics that distinguish it from other transformations. Within a single crystal (i.e., in a single grain in a polycrystalline material), the shear distortion occurs along a specific plane called the *habit plane*, which forms the interface between the martensitic and the austenitic phases. Since the habit plane does not rotate or deform during the course of the transformation, the plane is also referred to as the *lattice invariant plane*. Figure 1.16 schematically shows an austenite/martensite interface with its associated lattice invariant plane that separates austenite from a twinned martensite region. The transformation to martensite can occur along the lattice invariant plane by two different mechanisms, called *lattice invariant shear* mechanisms. The first one is through slip (i.e., atoms moving by one or more atomic space) and the second occurs by twinning (i.e., atoms moving through a fraction of an atomic space). Both of these mechanisms can aid formation of martensite with little or no volumetric change in the material. The strain obtained by such a cooperative movement of atoms is referred to as a *lattice invariant strain*.

In SMAs, twinning is the common mechanism of lattice invariant shear. The detwinning process results in a relative displacement of atoms that can eventually cause a macroscopic shape change while retaining their original

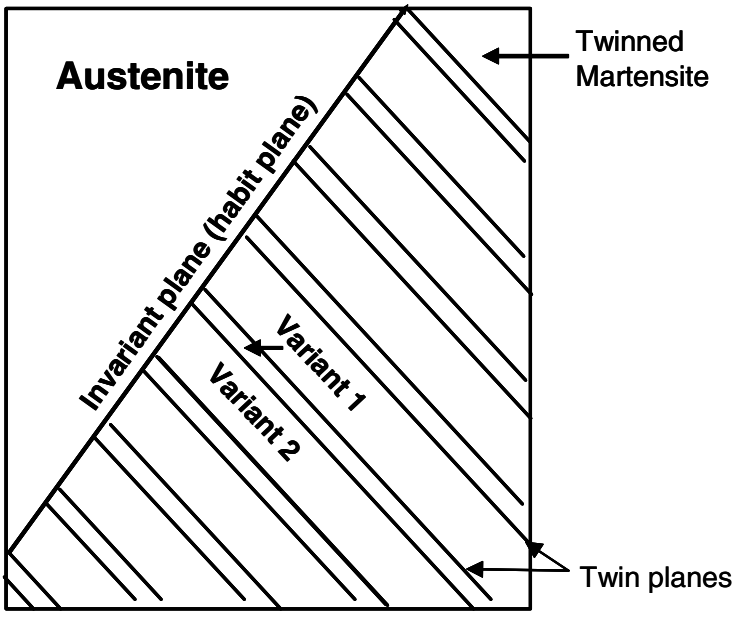

Fig. 1.16. Schematic of the austenite martensite interface.

atomic bonds, which also allows reversibility to the original crystallographic structure when heated to austenite.

Before proceeding with the detailed description of the transformation in SMAs, it is essential to have a preliminary understanding of the crystal structure of the associated phases. It is clear that there are two primary phases, austenite and martensite. The parent austenitic phase typically has a cubic (B2)[1] structure. The martensite that forms from austenite can have different crystallographic structures depending on the composition or the alloying element added. In equiatomic NiTi alloys for instance, the martensite that forms has a monoclinic (B19′) structure. Addition of an alloying element such as Cu or Pd can change the martensitic structure from a monoclinic to orthorhombic (B19), or create an intermediate R-phase (rhombohedral). In SMAs, during the transformation from austenite to martensite, every martensitic unit cell that forms can have different crystallographic orientations with respect to the cubic parent phase, and each unit cell having a different orientation is called a *variant*. Several such variants can form when the parent phase transforms to martensite. The number of variants that can form is dependent on the crystal structure of the martensite and its lattice correspondence with the parent phase unit cell.

An example of this can been seen in the NiTi system. Just as we have slip planes and slip systems in different crystal structures, there are "twin" planes along which twinning can occur. In the cubic lattice of the parent austenitic phase, the twinning shear can occur along the {011} planes to obtain the crystallographic equivalent martensite twins. Since there are six such {011} planes and two directions for the twinning to occur along each plane, there exist 12 equivalent martensitic twins. Each twin is composed of two martensitic variants, which, due to the shear distortion during transformation, assume a mirror symmetry. As a consequence of this, there are 24 total martensitic variants in most NiTi systems.

Recall that when austenite, under zero stress, transforms to twinned martensite, there is no associated shape change. The martensite that forms along the habit plane, under zero stress, occurs by twinning and the twins that form arrange themselves in a unique patterns to minimize the overall strain energy due to transformation. This behavior is familiarly known as the "self-accommodation" of twinned martensite.

An example of such a microstructure, as observed in NiTi is shown in Fig. 1.17[2]. In this micrograph three sets of twins A, B and C (six variants in total) together form a unique triangular morphology along the junction of three twin planes (the twin planes are shown by highlighted white lines).

[1] B2, B19′ and B19 are symbols that are partly systematic designations of the cubic, monoclinic and the orthorhombic crystal lattice structures respectively. This designation is known as the *Strukturbericht* designation.

[2] Reprinted from *Acta Materialia*, Vol. 45, Issue 12, Madangopal, K., pp. 5347–5365, Copyright 1997, with permission from Elsevier.

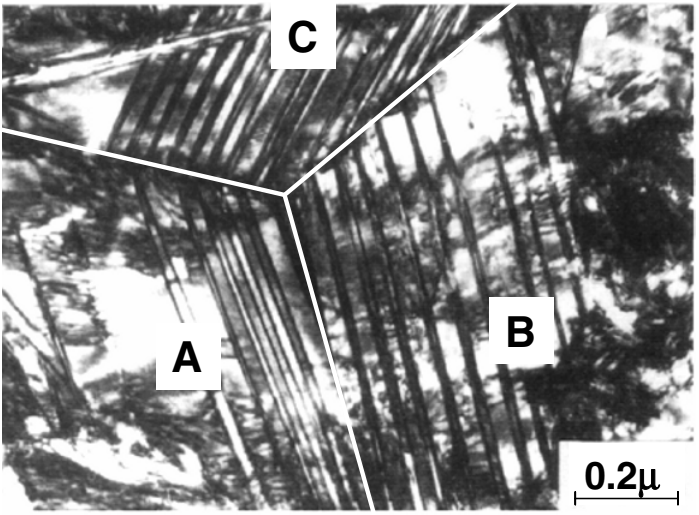

Fig. 1.17. Micrograph of self-accommodation monoclinic (B19′) structure in NiTi [31].

Similar to the self-accommodation as observed for the monoclinic structure, other martensitic crystal structures (i.e. orthorhombic, tetragonal, R-phase) can undergo self-accommodation. When the self-accommodated martensitic structure (monoclinic, orthorhombic or tetragonal) is subjected to an applied load, a resolved shear stress acts on the twin plane. When the resolved shear stress reaches a critical value, the most preferred variant (based on orientation to the applied stress) will evolve at the expense of other variants. This process of the evolution of the favorable variant and the associated generation of inelastic strain is known as the "detwinning" process. In the case of pseudoelasticity, a resolved shear stress reaches a critical value along the habit plane that leads to the formation of stress induced martensite.

The transformation from austenite to martensite and vice versa is associated with the release and absorption of latent heat. The heat of transformation and the associated transformation temperatures are most commonly determined using the *Differential Scanning Calorimeter* (DSC). The DSC is a popular thermal analysis technique that can be used to measure the phase transformation temperatures, the latent heat due to transformation, and the specific heat capacity of different phases in a material. This technique is also widely used to study the transformation temperatures of SMAs and has the advantage of requiring only a small quantity of material. The principle behind the operation of the DSC is the measurement of the rate at which heat energy is supplied to a specimen to maintain a constant heating or cooling rate. A DSC operating on such a principle is called a power compensated DSC. The device is termed differential because it has the ability to monitor the response

of two specimens and to subtract the results. This is most useful when a material specimen placed in a holding pan is loaded opposite an empty pan. The result of the differential scanning calorimetry is then the net response of the material sample only. The sample material can be encapsulated in an inert atmosphere to prevent oxidation.

Figure 1.18 shows a typical DSC curve for SMAs. The power (mW) required to maintain a constant heating or cooling rate for the SMA specimen is represented on the ordinate axis and the temperature of the chamber is shown on the abscissa axis. When the specimen is heated from the twinned martensitic state, the transformation to austenite initiates at A_s. The endothermic reaction during the reverse transformation requires that additional heat power be supplied to the specimen to maintain the prescribed constant heating rate. This change in the power supplied as the temperature increases is recorded as a transformation "peak" during heating. A similar peak is also recorded during the cooling process during which the exothermic transformation from austenite to martensite takes place. The transformation temperatures from the acquired data are generally measured by drawing tangents to the start and end regions of the transformation peak and the baseline of the heating and cooling curves. The specific heat capacity can be computed by normalizing the power by the heating rate and the weight of the specimen. The associated latent heat for phase transformation can be calculated by integrating the specific heat over the range of the transformation temperatures. Most DSC software packages include the provision to directly compute the latent heat due to transformation.

The transformation temperatures can also be significantly affected by stored mechanical energy (i.e. precipitates, dislocations introduced due to processing/cutting, detwinning), therefore making the initial state of the material very important. This stored mechanical energy can cause a shift in and/or widen the transformation temperatures, or even cause an intermediate phase

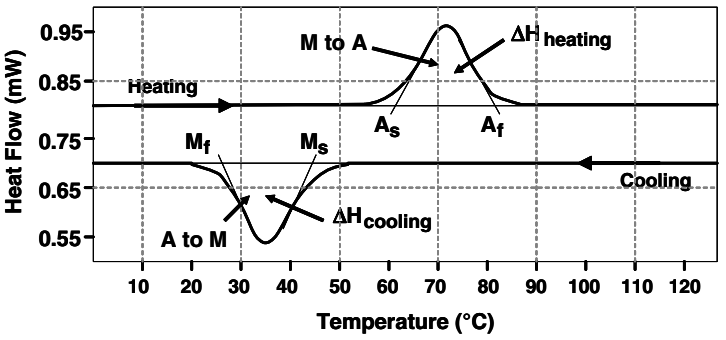

Fig. 1.18. A schematic of a DSC curve for an SMA showing the transformation temperatures and the associated latent heat of transformation during heating and cooling.

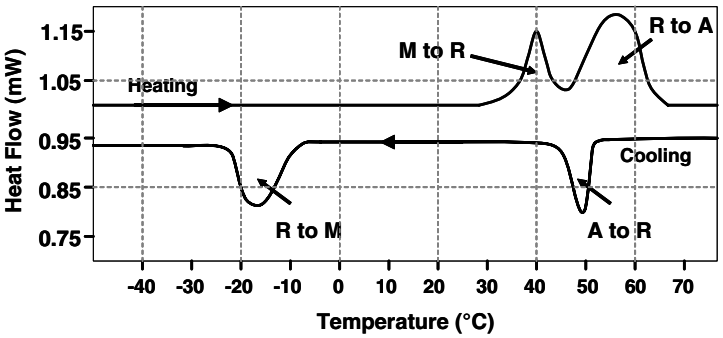

Fig. 1.19. A DSC curve for a Ni-rich NiTi SMA showing the two-stage transformation from austenite to martensite.

transformation. A DSC curve of a Ni-rich SMA showing an intermediate phase, called the R-phase, in the cooling curve is shown in Fig. 1.19. Further details about the R-phase will be discussed in Section 1.9.

1.9 Effect of Alloying on the Transformation Behavior of SMAs

Starting from the initial investigation of AuCd and AgCd alloys in the 1930s, to the discovery of Nitinol in 1963, and to the newest compositions being researched today, a wide variety of SMAs have been investigated over the last seven decades. New compositions have been fabricated by adding different alloying elements to existing alloys, providing a catalog of SMAs with a variety of properties to choose from. Such a wide selection gives designers great flexibility in tailoring SMA properties to match the constraints of a given commercial application. Shape memory alloys can be classified based on a wide variety of categories: primary alloying elements, mode of actuation (magnetic, thermal), operating temperature, or desired behavior. Some of the most commonly used SMAs, their properties, and the effect of alloying on them are discussed in this section.

1.9.1 NiTi-Based Alloys

Of the known SMA compositions, the NiTi alloy system has been studied most extensively and is used in the greatest number of commercial applications. This alloy exhibits strong SME, TWSME, and pseudoelastic behavior under the right conditions, which makes this material ideal for a variety of applications. It also exhibits resistance to corrosion and is biocompatible, making it suitable for use in biomedical applications. Compared to the less widely used alloys, the crystallography and thermomechanical response of NiTi are

well understood, as are the the effects of heat treatment and the variation of transformation temperatures with changes in composition. In this section we briefly discuss the NiTi system, including the NiTi based ternary alloys.

NiTi - In the early 1960s, Buehler and his coworkers discovered the shape memory effect in an equiatomic NiTi alloy [7, 32]. The equiatomic composition (i.e. 50 at% of Ni and Ti) exhibits the maximum A_f temperature (120 °C) of all NiTi compositions studied. Decreasing the Ni atomic percentage (at.%) from the equiatomic composition does not change the transformation temperatures. If the composition of nickel is increased above 50 at.%, the transformation temperature begins to decrease, with A_f becoming as low as −40 °C for 51 at.% nickel. This variation in composition can change the ambient room temperature (23 °C) characteristics from SME to pseudoelasticity.

In Ni-rich alloys, aging at the temperature of 400 °C results in the formation of lenticular Ti_3Ni_4 precipitates. The stress fields due to the precipitates formed can result in the formation of an intermediate phase known as the *R-phase* between the austenite and martensite phases. The name "R-phase" is associated with the rhombohedral structure of the crystal. This phase generally vanishes with heat treatments at high temperatures and thus its existence is associated with certain specific conditions [33]. These conditions include substituting small amounts of Ni with Fe or Al, stress fields due to precipitates in Ni-rich NiTi, and stress fields due to dislocations in cold worked/heat treated alloys. NiTi alloys exhibit fully recoverable transformation strains of up to 8% and can be commercially obtained in various forms (e.g., wires, strips, rods, tubes and plates).

Recent studies have also investigated 55 at.% NiTi composition [34]. This composition exhibits transformation temperatures in the range of −10 °C to 60 °C. The alloy is a chemically multi-phased alloy, which is one of the primary reasons why it exhibits low transformation strains. However, 55 at.% NiTi alloy has been proven to show superior corrosion resistance as compared to stainless steels in harsh environments such as a salt water bath or salt fog [35]. The alloy also shows excellent thermomechanical stability, easier control of transformation temperatures through heat treatment, and can be hot formed into various complex shapes as these alloys do not require cold working [36, 37].

NiTiCu - The addition of Cu to NiTi preferentially replaces Ni to form NiTiCu alloys. The unique property of these alloys is that addition of Cu reduces the hysteresis of the SMA response. However, this also results in a decrease in the transformation strain. In NiTi 10 at.% Cu, the transformation hysteresis is much smaller than for the binary alloy at the expense of the total transformation strain which is reduced to approximately 4.0% [38]. The addition of Cu also reduces the pseudoelastic hysteresis. The width of the pseudoelastic hysteresis is less than 100 MPa for NiTi 10 at.% Cu when compared to a width greater than 200 MPa for the binary alloy. The addition of Cu to the binary alloy also greatly reduces the sensitivity of the martensitic start temperature to composition [39]. This change in the material behavior is associated with the change in the phase transformation. Studies on the phase

transformation behavior of the NiTiCu system have shown that for a composition of 7.5 at.% ≤ Cu ≤ 15.0 at.%, the material undergoes a clear three stage cubic to orthorhombic to monoclinic transformation [40]. The low stress level required to transform the cubic phase to the orthorhombic phase results in the lowering of detwinning stress level.

The small hysteresis associated with the transformation makes TiNiCu an ideal choice for actuators. Among the different compositions of TiNiCu, 5.0 at.% ≤ Cu ≤ 10.0 at.% is most preferred. Addition of Cu greater than 10 at.% embrittles the material. Recent studies [41] on 25 at.% Cu fabricated by the melt spun technique have shown to have small hysteresis and stable pseudoelastic total strains of up to 7.0 %. DSC and Transmission Electron Microscopy (TEM) studies of this composition have also shown the $B19 \rightarrow B19'$ transformation occurring in the material [42].

NiTiNb - Unlike actuation devices that require a small hysteresis, a device used for the purpose of coupling must meet a different set of requirements in terms of SMA properties. One such requirement would be for the material to show minimal response to wide temperature changes. This can be achieved by widening the hysteresis of binary NiTi. The alloying element that facilitates this characteristic is Niobium (Nb). The effect of adding Nb was first studied in 1986 [43, 44]. It was noted that one consequence of adding Nb to NiTi was the widening of the thermal hysteresis. The wide hysteresis has important practical use in the field of SMAs, facilitating the engineering of material properties for which room temperature lies within the regions of the hysteresis. This allows the material to be deformed at low temperatures and yet be safely transported at ambient temperatures.

In the early work on $Ni_{47}Ti_{44}Nb_9$ [45], it has been shown that the alloy primarily consists of the NiTi phase with dispersed insoluble elliptical or globular precipitates of nearly pure Nb. These precipitates are extremely soft with a deformation stress equivalent to the detwinning stress of martensite. The large thermal hysteresis of the material is associated with the partitioning of the strain into a recoverable part (due to the NiTi phase) and an irrecoverable part (due to the Nb precipitates). This also explains why the material does not exhibit complete recovery during the deformation, and why a deformation corresponding to approximately 4 % strain can induce permanent strain in the material. Techniques such as pre-deformation can further increase the hysteresis width in these alloys by increasing the A_s temperature [46, 47]. Newer compositions with lower Nb concentration (3 at.%) have shown promising SME behavior [48].

NiTiX (X = Pd, Pt, Hf or Zr) alloys - Development of SMAs for commercial applications over the last four decades has primarily concentrated on applications with operating temperatures ≤ 100 °C. However applications involving high operating temperatures, such as in the core region of an aircraft engine or down hole applications in the oil industry require SMAs with high transformation temperatures and stable material properties. This demand for SMAs with high transformation temperatures has led to the development

of a new class of SMAs known as *High Temperature Shape Memory Alloys* (HTSMAs). HTSMAs are a unique class of SMAs that have transformation temperatures greater than 100 °C and are capable of actuating under high temperature conditions. These alloys are produced by adding ternary elements such as palladium, platinum, hafnium, gold, and zirconium to NiTi, for which the transformation temperatures can be shifted anywhere in the range of 100–800 °C [4, 49, 50].

Similar to conventional SMAs, HTSMAs have austenitic and martensitic phases that can transform from one state to the other. The earliest studies on HTSMAs were performed in 1969 [12] on alloys such as Au-Ti, Pd-Ti and Pt-Ti to investigate whether these materials undergo martensitic transformation similar to (Au, Ag)-Cd alloy systems. In these studies, it was also revealed that these materials exhibit very high transformation temperatures. In 1981, detailed studies were performed on the TiNiPd alloy system, and it was determined that the temperatures for phase transformation were composition dependent [51]. Since then, several studies have been performed on TiNiPd, TiNiPt and TiNiAu alloy systems [49, 52]. Recent studies on various compositions of TiNiPd and TiNiPt alloys have investigated the work characteristic and workability of these materials [53, 54]. However, due to the extremely high cost associated with palladium and platinum, such alloys have limited commercial viability. Other alloy systems, such as TiNiHf [50] and TiNiZr [55], are also being widely investigated. Although these materials do not possess transformation temperatures as high as NiTiPd and NiTiPt, they are more cost effective. The primary limitations of HTSMAs are that the transformation strains associated with the material are approximately 3%, and that these materials have a low critical stress for slip. A sampling of NiTi-based ternary alloys and their associated transformation temperatures is shown in Table 1.1. Note that these values are highly dependent on material history, including heat treatment, and are given to indicate general trends.

1.9.2 Copper-Based Alloys

Although NiTi SMAs offer excellent pseudoelastic and SME properties and are biocompatible, they are relatively expensive compared to Cu-based SMAs. Good electrical and thermal conductivity along with their formability makes Cu-based SMAs an attractive alternative to NiTi. Copper-based alloys generally exhibit less hysteresis than NiTi, with the transformation temperatures in Cu-based alloys highly dependent on the composition. A precise change from 10^{-3} to 10^{-4} at.% is sometimes necessary to achieve reproducible transformation temperatures within a 5 °C range. The main Cu-based alloys are found in the Cu-Zn and Cu-Al systems. In this section some of the most commonly used Cu based SMAs will be discussed.

CuZnAl - The CuZn binary alloys are very ductile and have resistance to intergranular fracture as compared to other Cu-based alloys [5]. These alloys

Table 1.1. Representative transformation temperatures for SMAs with different compositions and heat treatments.

NiTi Based SMAs	M_f	M_s	A_s	A_f	Reference
$Ti_{50}Ni_{50}$	15	55	80	89	[49]
$Ti_{49.5}Ni_{50.5}$	−78	−19	9	53	[56]
$Ti_{49}Ni_{51}$	−153	−114	−89	−40	[4]
$Ti_{49}Ni_{51}Cu_{10}$	8	30	35	50	[56]
$Ti_{50}Ni_{40}Cu_{10}$	21	41	53	67	[56]
$Ti_{44}Ni_{47}Nb_9$	−175	−90	−85	−35	[45]
$Ti_{42.2}Ni_{49.8}Hf_8$	50	69	111	142	[57]
$Ti_{40.7}Ni_{49.8}Hf_{9.5}$	61	90	118	159	[57]
$Ti_{40.2}Ni_{49.8}Hf_{10}$	103	128	182	198	[57]
$Ti_{35.2}Ni_{49.8}Hf_{15}$	95	136	140	210	[57]
$Ti_{30.2}Ni_{49.8}Hf_{20}$	127	174	200	276	[57]
$Ti_{48}Ni_{47}Zr_5$	20	65	75	138	[58]
$Ti_{43}Ni_{47}Zr_{10}$	45	100	113	165	[58]
$Ti_{38}Ni_{47}Zr_{15}$	100	175	175	230	[58]
$Ti_{33}Ni_{47}Zr_{20}$	205	275	265	330	[58]
$Ti_{50}Pd_{50}$	550	563	580	591	[49]
$Ti_{50}Ni_{20}Pd_{30}$	208	241	230	241	[49]
$Ti_{50}Ni_{10}Pd_{40}$	387	403	419	427	[49]
$Ti_{50}Ni_5Pd_{45}$	467	486	503	509	[49]
$Ti_{50}Ni_{45}Pt_5$	10	29	36	49	[49]
$Ti_{50}Ni_{40}Pt_{10}$	−8	18	−27	36	[49]
$Ti_{50}Ni_{30}Pt_{20}$	241	300	263	300	[49]
$Ti_{50}Ni_{20}Pt_{30}$	537	619	626	702	[49]

transform to the martensitic state at a temperature below room temperature. Addition of aluminum to the binary alloy can considerably increase the transformation temperatures. Varying the composition of aluminum between 5 wt.% and 10 wt.% can shift the M_s temperature from −180 °C to 100 °C. However, the parent phase exhibits a strong tendency to decompose into its equilibrium phases when overheated or aged. Due to this, the operating temperatures are typically restricted to approximately 100 °C. The transformation temperatures of the alloy are extremely sensitive to composition, and zinc can be lost during the melt process. Due to these factors, the fabrication process of the alloy needs to be precisely controlled. CuZnAl alloys are also very sensitive to heat treatments such that the quenching rate can lead to phase dissociation or change in transformation temperatures. Their mechanical behavior is limited to stress levels of approximately 200 MPa due to the low critical stress for slip. Within the operational range of stress, the alloy exhibits perfect SME and pseudoelasticity, but the transformation strain is limited to about 3-4% [5]. Since CuZnAl is very ductile as compared to other Cu-based alloys, they are mostly chosen for use in applications.

CuAlNi - CuAlNi is less sensitive to stabilization and aging phenomena. Similar to CuZnAl, the transformation temperatures of CuAlNi can be varied by changing the aluminum or nickel content. Changing the aluminum composition between 14 at.% and 14.5 at.% can change the M_s temperature from $-140\,°C$ to $100\,°C$. The relative change in transformation temperatures is not significant and the hysteresis remains fairly constant. Since this alloy is harder to produce, manganese is often added to improve its ductility and titanium is added to refine its grains. However, the primary limitation of the CuAlNi system is the poor ductility due to intergranular cracking [4]. This phenomenon also affects the mechanical behavior such that the material typically fractures at a stress level of about 280 MPa. Transformation strain in these materials is limited to 3%. The material also exhibits very poor cyclic behavior [4].

Developed later (1982), the CuAlBe alloy has been studied during the last few years. Recently, several other Cu-based SMAs are in development, such as CuAlMn which has good ductility and CuAlNb which is suitable for high temperature applications.

1.9.3 Iron-Based Alloys

FeNiCoTi and FeMnSi are the main ferrous SMAs. $FeNi_{31}Co_{10}Ti_3$ after specific thermomechanical treatment, exhibits SME. The alloy exhibits a thermal hysteresis of approximately 150 °C.

Another ferrous alloy with good commercial prospects is FeMnSi. Si is primarily added to improve the shape memory effect and raise the critical stress for slip in austenite. When subject to training under a specific thermomechanical loading path, these SMAs exhibit complete SME. The transformation strains in these alloys are in the range of 2.5-4.5% [5].

1.9.4 Additional SMAs

CoNiAl - CoNiAl alloys are created by addition of Co to NiAl or Ni to the CoAl binary alloy systems, both of which exhibit very good corrosion and oxidation resistance at high temperatures. The CoNiAl alloy undergoes a transformation from the parent cubic structure phase to a tetragonal martensitic phase. Although the martensitic transformation in this alloy system was discovered as early as 1971 [59], the alloy system was not extensively investigated due to its brittle nature. However, recent efforts of forming and controlling the quantity of intermetallic phases by heat treatments has helped improve the ductility of the material [60, 61]. A typical composition of $CoNi_{33}Al_{29}$ has transformation temperatures of M_f approximately $-57\,°C$ and A_f approximately $-26\,°C$. The material also exhibits a transformation strain of approximately 4.0% due to thermal cycling. In addition, the pseudoelastic behavior of the alloy has shown stability over a temperature range of 150 °C above A_f [62]. While the conventional SME and pseudoelastic behavior in this ternary alloy has been

investigated, the CoNiAl composition has also been widely studied for its magnetic properties and the possibility of a magnetic-field-induced re-orientation. In such a transformation, the martensite reorients when subject to an external magnetic field. As a result, the material generates a magnetic-field-induced reorientation strain. Further, these materials can operate at much higher actuation frequencies ($\simeq$ 1 kHz) as compared to thermally activated SMAs. Studies on $CoNi_{33}Al_{29}$ have shown the material to exhibit strains of 0.06% due to magnetic field reorientation [63].

NiMnGa - The most widely investigated *Magnetic Shape Memory Alloys* (MSMAs) are NiMnGa alloys. The first conclusive report of martensitic transformations in Ni_2MnGa alloys was given in 1984 [64]. However, it was only in 1996 that the first suggestion on the possibility of a magnetic field-controlled shape memory effect in these materials was made [15]. A field induced reorientation strain of nearly 0.2% was observed in the stress-free experiments on martensitic Ni_2MnGa single crystals. Further work on off-stoichiometric intermetallic compounds near the composition Ni_2MnGa, in combination with thermomechanical treatments and the utilization of a better understanding of the crystallographic structure of these alloys, have yielded larger field-induced strains of 6% [65], and up to 10% [66, 67], in single crystals. The main limitation of Magnetic Shape Memory Alloys (MSMAs) is the relatively low blocking stress (the stress at which the magnetic reorientation strain is completely suppressed). The typical blocking stress level for MSMAs is 6-10 MPa. Ni_2MnGa also undergoes the typical pseudoelastic transformation with compressive strains of up to 4.0%. Recent studies have shown that a unique combination of the pseudoelastic transformation behavior combined with a magnetic field can produce a field induced phase transformation of approximately 0.5%. This field induced transformation has also increased the blocking stress of the material to 20 MPa [68].

Other magnetic shape memory alloys have been studied including Fe-Pd [69–72], Fe-Ni-Co-Ti, Fe-Pt, Co-Ni-Ga, Ni-Mn-Al [73–75], and Co-Ni-Al [63]. These alloys exhibit lower field-induced strains, but can have other advantages. The largest field-induced strains that have been observed in Fe-Pd, for example, reach 3.1% [76]. Fe-Pd, however, is more ductile than Ni-Mn-Ga [69]. A much more detailed explanation of the magnetic field induced reorientation and transformation behavior will be discussed in Chapter 7.

1.10 SMAs as Active Materials — Applications

Active materials are quickly gaining the attention of engineers and scientists worldwide as more emphasis is placed on both reliability and multifunctionality. For the past several decades, engineers and other designers in many fields have been developing ways to convert thermal energy into mechanical work through the use of SMAs and apply these solutions to real-world applications. One of the most well-known examples was the

hydraulic tube coupling used on the F-14 in 1971 [77]. Since then engineers in various industries have continued to use the unique properties of SMAs in solving engineering problems. SMAs have attracted a great deal of interest in various fields of application ranging from aerospace [78] and naval [79] to surgical instruments [80], medical implants and fixtures [81]. This section reviews some of the applications of SMAs in these different fields.

1.10.1 Aerospace Applications

SMA technology implementation in the aerospace industry has spanned the areas of fixed-wing aircraft, rotorcraft, spacecraft and work in all these areas is still progressing. Some of the more recent applications of SMAs and research on their potential uses in these areas are described in the following sections.

Fixed-Wing Aircraft Applications - Perhaps two of the most well-known fixed-wing programs are the Smart Wing program and the Smart Aircraft and Marine Propulsion System demonstration (SAMPSON) [82]. The Smart Wing program represented a collaboration between DARPA, AFRL, and Northrop Grumman, and its purpose was to implement active materials, such as SMAs, to optimize the performance of lifting bodies [83]. In this program, SMAs were used as wire tendons to actuate hingeless ailerons and were also formed into torque tubes that initiated spanwise wing twist of a scaled-down F-18 aircraft wing. Although satisfactory actuation was provided by the SMAs at 1:6 scale, it was found that the SMA torque tube was not strong enough to actuate a full-scale wing. The as-tested torque tube installation is shown in Fig. 1.20.

There have been a number of other efforts to integrate SMA elements into aerostructures. One such study led to the development of a variable geometry airfoil. Through SMA actuation, this airfoil effectively changed its configuration from symmetric to cambered [84]. Many other studies on the utilization of SMAs in aerostructures have focused on actuating smaller elements. SMAs can be used in smaller elements because their behavior is exhibited across a large range of sizes. One includes looking into the possibility of pairing SMAs and Micro-Electromechanical Systems (MEMS) to decrease the turbulent drag of an aerodynamic surface [85]. When activated appropriately, the MEMS skin would create a traveling wave to energize the boundary layer and thereby decrease turbulent drag. Some research has also been performed in the area of dynamic property optimization of aircraft structural panels using SMA elements, which provide a changing elastic stiffness via the martensitic transformation. It was found that the thermally-induced post-buckling deflection of a structure could be decreased by pre-straining the SMA or increasing the volume fraction of the SMA fibers [86]. The concept of a tunable SMA "Smart Spar" represented another attempt to alter the dynamic properties [87].

The usefulness of active materials in tailoring propulsion systems was demonstrated through the SAMPSON program [88]. One of the uses of SMAs in this program was to change the geometry of an F-15 engine inlet. This

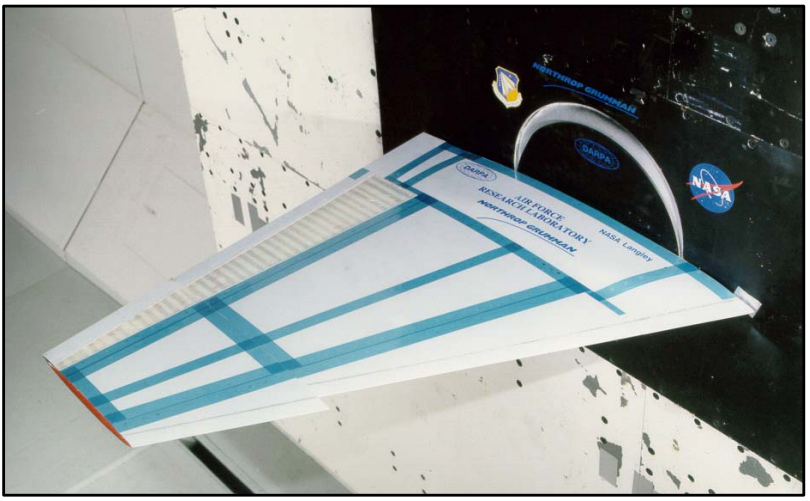

(a)

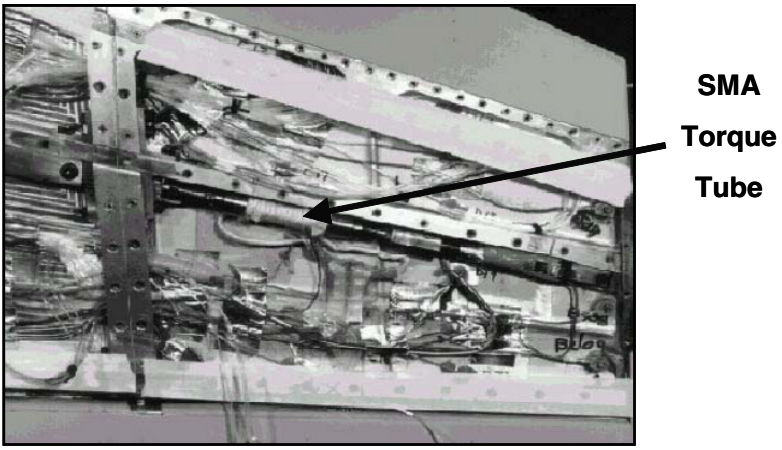

(b)

Fig. 1.20. (a) Total view of the SMART Wing model. **(b)** Cut away view of the SMA torque tubes as installed in the model during Phase 1 of the SMART Wing project [82].

experiment was done on a full scale inlet and the experimental setup can be seen in Fig. 1.21[3] [89]. A total force of approximately 26,700N was achieved through the use of SMA bundles containing 34 wires/rods. This generated

[3] Reprinted from *Journal of the Minerals, Metals, and Materials Society*, Vol. 55, No. 12, Wax, S.G., Fischer, G.M., and Sands, R.R., pp. 17–23, Copyright 2003, with kind permission from Springer Science and Business Media.

Fig. 1.21. The SAMPSON F-15 inlet cowl as installed in the NASA Langley Transonic Wind Tunnel [82, 89].

force rotated the inlet cowl through 9°. Another concept tested by the SAMPSON program was the concept of changing the shape of the inlet lip through a more complex system of SMA actuation.

Engine noise levels during take off and landing have become more highly regulated worldwide. To reduce this noise, some designers are installing chevrons onto engines to mix the flow of exhaust gases and reduce engine noise. Research is being performed into methods by which SMA beam components can be embedded inside chevrons. The SMA beams bend the chevrons into the flow during low-altitude flight or low speed flight, thereby increasing mixing and reducing noise. During high-altitude, high speed flight, these

Fig. 1.22. Boeing variable geometry chevron, flight testing [92].

SMA beam components will cool into martensite, thereby straightening the chevrons and increasing engine performance [90]. The current Boeing design for these variable geometry chevrons can be seen in Fig. 1.22.

A different solution to the active chevron problem has been proposed by NASA. In this design, SMA strips are installed on each side of the chevron centroid during the fabrication process [91]. Upon heating, the SMA strips contract alternately, leading to asymmetric stresses within the chevrons and therefore create a bending moment.

Rotorcraft - The role of SMAs in rotorcraft applications has been focused on the main rotor [93]. One active research area is SMA blade twist actuation [94]. SMAs are ideally suited for such applications because of their high actuation energy density and forces required in the small available volume within a rotor blade. One study proposed the use of SMA torque tubes to vary the twist of rotor blades, as found on tiltrotor aircraft [95]. These SMA torque tubes, when actuated, could facilitate the formation of different blade configurations and thereby optimize performance of such aircraft in both the hover and forward flight regimes. Recent work has also been performed on developing SMA-actuated tabs to improve tracking [96]. A trailing edge tab actuated by SMA wires was built into an airfoil section to accomplish this improvement. Alternately, the Smart Material Actuated Rotor Technology (SMART) Rotor project team [97] proposed to link an SMA torque tube to the tracking tab. Other rotorcraft applications include using SMA wire components for collective control [98] and to provide rotor blade tip anhedral [99],

which minimized the blade vortex interaction noise by moving the blade tip vortex away from the rotor plane.

Spacecraft Applications - SMAs have been used in space applications to address problems related to actuation and release in zero atmosphere environment as well as vibration damping during spacecraft launch. Most of the applications and systems are typically designed by careful experimentation. One such application that uses SMAs is for the low-shock release mechanism in satellites [100]. Until 1984, it was estimated that nearly 14% of space missions experienced failure due to shock, and, in some cases, caused the mission to be aborted [101]. The shocks were caused due to pyrotechnic release mechanisms. The slow actuation due to gradual heating in SMAs makes them suitable for low shock release mechanisms in space applications. The scalability of SMA actuator designs also facilitates fabrication of smaller release devices for smaller satellites [102] in need of compact release mechanisms. Some of the devices developed for this purpose include the Qwknut [103] and the Micro Sep-Nut [102]. In both of these devices, the shape memory effect is used. Another miniature release device for space applications utilized a rotary actuation. The device, with a maximum dimension of 5mm, could provide a rotary actuation through an angle of 90°.

SMAs are also used in actuation of various components such as solar panels. An early design of this used SMA torsional elements to actuate solar collectors [93]. The Lightweight Flexible Solar Array (LFSA) [104] used thin SMA strips as hinges, which deploy the folded solar panels upon heating in approximately 30 seconds. The proof of concept design is shown in Fig. 1.23.

A different SMA space actuation application was utilized on the Mars Pathfinder mission in 1997. An SMA actuator was used to rotate a dust cover from a specific region of a solar cell so that the power output of this protected,

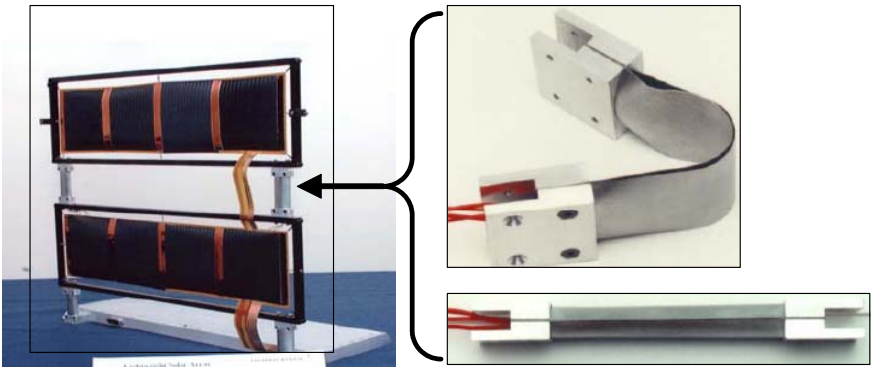

Fig. 1.23. The LFSA and the SMA hinges shown in the folded and the deployed configurations [104].

and therefore clean area of the panel could be compared to the power output of non-protected regions. This determined the negative effects of dust settlement on the solar panels. In addition to actuation, another attractive application for SMAs is vibration isolators and dampeners [101]. The hysteresis in the pseudoelastic behavior is representative of the mechanical energy that an SMA can dissipate during a cycle. Further, the change in the stiffness from the initial elastic region to that in the transformation region makes it an effective tool to isolate vibrations.

1.10.2 Medical Applications

The shape memory and pseudoelastic characteristics coupled with the biocompatibility of NiTi make them an attractive candidate for medical applications. The combination of these unique characteristics has led to the development of various applications such as stents, filters, orthodontic wires as well as devices for minimally invasive surgery (MIS).

An important requirement for an SMA, or any other material to be used in the human body, is that it be biocompatible. Biocompatibility is a property of the material to remain nontoxic through its functional period inside the human body. A biocompatible material can not produce any allergic reaction or inflammatory response in the host. The other requirement for the material is its biofunctionality, which is the ability to function desirably for its expected service life in the human body environment. These two requirements are crucial for the application of SMAs in the medical industry.

Several investigations have been performed to study the biocompatibility and biofunctionality of NiTi alloys [105, 106]. Analysis has focused on each individual element that constitutes the alloy, namely, nickel and titanium. Nickel intake occurs in a regular lifestyle [107], and most often its impact at trace levels is minimal. However, excessive intake of nickel can be poisonous to the human body. Unlike nickel, titanium and its compounds are intrinsically biocompatible and are commonly used in orthopedic and orthodontic implants [108]. The oxidation of titanium results in a coating of TiO_2, which provides a corrosion-resistant layer, making such a device stable within the human body. Corrosion studies performed on NiTi alloys have shown better stability than most alloys used in medicine and dentistry [109]. It has also been shown that surface coating NiTi with TiN or TiCN is effective in further improving the corrosion resistance of this material.

Orthodontic Applications - The properties of SMAs have been successfully implemented in a variety of dental applications. Nitinol orthodontic archwires have been used since the 1970s [110], and are more effective than other alternative materials. In a linear elastic material like stainless steel, there is a large increment in stress, for a small increment in strain which results in a large amount of force on the tooth for a small amount of corrective motion. The advantage of pseudoelastic arch wires is the ability to operate in the pseudoelastic plateau, during which the material has a near-zero stress change over

a large strain increment. As a result, they provide a nearly constant, moderate force to actively move the teeth over a longer period of time compared with stainless steel. Further, the material composition and processing can be engineered to produce different levels of optimal force. An example of Nitinol orthodontic braces is shown in Fig. 1.24a.

Another key dental application for SMAs involves the use of Nitinol drills used in root canal surgery, which involves careful drilling within the tooth (Fig. 1.24b). The advantage of these Nitinol drills is that they can bend to rather large angles, which induce large strains, yet still withstand the high cyclic rotations [111].

Cardiovascular Applications - An early cardiovascular SMA device was the Simon Filter. The device acts as a filter that traps clots traveling in the blood stream. The trapped clots are then eventually dissolved. From the original expanded state, the device is deformed and constrained within a catheter. At the time of implantation, the filter is deployed in the blood vessel where the ambient temperature exceeds A_s of the filter material. The release from the constraint and the active properties of the SMA filter cause the filter to expand and it assumes its original shape as shown in Fig. 1.25a [112].

Another application of SMAs in the cardiovascular field is the atrial septal occlusion device. This device is used to seal an atrial hole that is located on the surface dividing the upper heart chambers. The traditional surgical technique used to address this problem is highly invasive and dangerous. The atrial septal occlusion device provides a suitable alternative to such a surgery. This device also exploits the shape memory characteristics exhibited by SMAs, and consists of two umbrella shape halves that can be screwed together in the center. Initially, these halves are folded, constrained and introduced into the heart. The two halves are deployed on either side of the hole and are connected using a screw. The resulting "sandwich" configuration forms a patch that seals the hole.

(a)

(b)

Fig. 1.24. Orthodontic application of SMAs: (a) Nitinol braces used for alignment purposes in dental applications. (b) A schematic showing a NiTi drill used for root canal surgery.

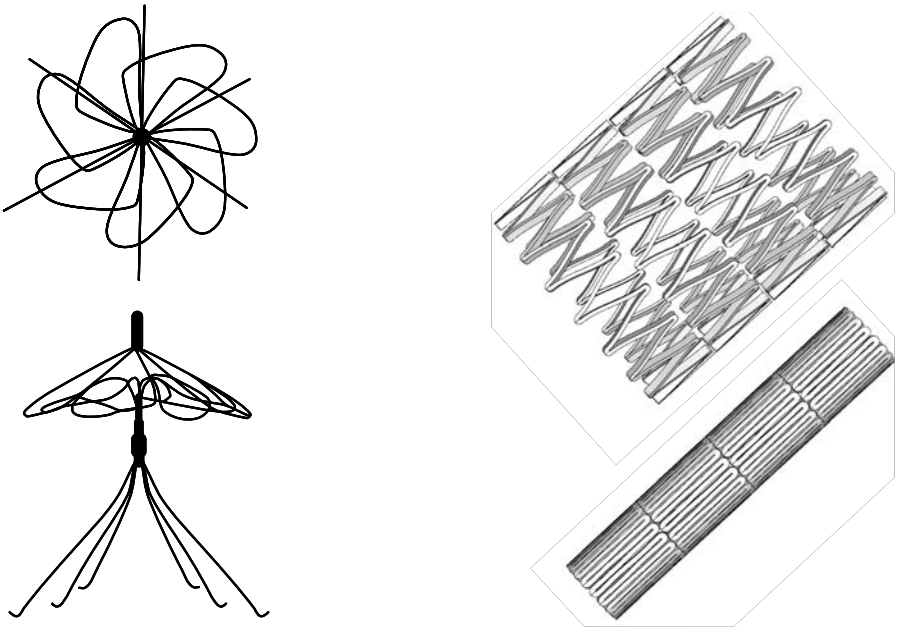

(a) (b)

Fig. 1.25. Cardiovascular devices that utilize the engineering properties of SMAs: (a) Top view (above) and side view (below) of the Simon filter in the deployed configuration [112]. (b) A self-expanding Nitinol stent shown in the deployed configuration (above) and constrained state (below).

A more common cardiovascular application is the "self-expanding" NiTi stent. Like other conventional stents, this device is used to support the inner circumference of tubular passages in the body such as blood vessels. Traditionally, stents are made using stainless steel. These stents are expanded from the size of the introduced catheter to the size of the artery walls by an inflatable balloon. As the balloon is deflated, the steel stent undergoes elastic unloading, often resulting in a loose fit. Furthermore, to reach a particular nominal diameter, it is necessary to over-expand the stent to account for this unloading. This process of over-inflation can damage the vessels and can cause a condition where the blood vessel collapses after the procedure due to weakening of the walls. The self-expanding NiTi stents provide an attractive alternative to the traditional method. The device is generally laser cut from sheets or tubing and is then shape set to the appropriate diameter. After being constrained, the NiTi stent is introduced into the body where the temperature exceeds A_s of the stent material. It is then released in the artery where it expands to its original larger diameter and gently pushes outward on the walls. Furthermore, the device can adapt to any oblong passage as compared to the balloon inflated steel stents that are biased towards a circular shape. Fig. 1.25b shows

an illustration of a Nitinol stent in the constrained and deployed configuration. Engineering analysis of such a device will be considered in Chapter 4.

Orthopedic Applications - The devices developed for orthopedic applications are used to support injured, weakened or fractured bones. One such device is the spinal vertebra spacer (Fig. 1.26a), used to provide local reinforcement to the vertebrae and prevent motion during the healing process. The device applies a constant force on the joint while providing flexibility [107].

Porous SMAs represent a different kind of material form and can be used as artificial bone implants (Fig. 1.26b) [113]. The porous nature of the material enables the existing bone tissue to migrate inward, increasing bonding strength. Furthermore, the implant properties (stiffness and porosity) can be engineered to match those of the bone. In a separate application, SMAs fasten to broken or fractured bones to facilitate healing. These devices include orthopedic staples and shape memory plates. The staple, for example, is installed in an open configuration at the fractured joint. An external heating source is used to heat the staple causing it to return to its original form via SME, which consequently provides a compressive force at the interface of the separated bones [107]. The shape memory plate is a device used when a cast cannot be applied over the fracture surface (i.e. facial areas, jaw, nose). The plate is also "shape set", deformed, installed and then actuated via (external) heating, providing a force which holds the fractured joints together [107].

Surgical Instrument Applications - Advances in medicine continue to enhance the use of minimally invasive surgery (MIS). Some of the enabling technologies advancing MIS includes instruments that can be inserted through these small openings followed by expansion to a desired size for the particular function. The pseudoelastic and shape memory effect properties of SMAs allow for more creative design options compared to conventional materials. One such device is the SMA basket used to remove stones in the bile duct. Other instruments using the shape memory effect behavior include surgical tools with grippers, scissors and tongs used in laparoscopy procedures. Pseudoelastic guide wires are widely used in surgery due to their kink resistance and superior flexibility [112].

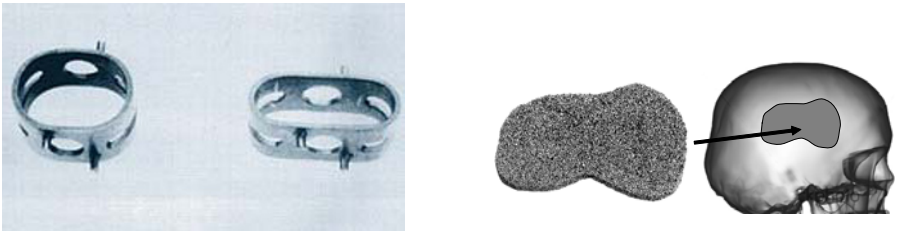

(a) (b)

Fig. 1.26. Orthopedic applications of SMAs. **(a)** Spinal vertebrae spacers showing the device in the martensitic and the deployed austenitic state [112]. **(b)** A schematic showing the prospective use of porous SMAs as artificial bone implants.

1.10.3 Transportation Applications

Shape memory alloys have been used in automobiles for applications ranging from impact absorption to sensing and actuation. The pseudoelastic behavior hysteresis provides an effective system to dissipate vibrations and impact. This property has been used for impact absorption on armor vehicles in military [114] and commercial applications [115]. One design for an impact absorption application required the deployment of a protective panel within 5-7 ms. The limited response time of commercially available actuation devices (10 ms) is overcome by the use of an SMA element. The device can be released in 3 ms and then reset for another actuation. The SME has also been implemented for actuating blinds that cover the fog lamp to prevent damage. A series circuit ensures the actuation of the SMA louvers every time the fog lamps are turned on. SMAs can also be used for sensor and actuation purposes simultaneously. An application that exploits this behavior is the SMA spring for the continuous variable transmission in the Mercedes A class. The spring acts as a sensor that monitors the temperature and actuates a valve at a specific temperature, which changes the direction of oil flow.

A similar actuation system is incorporated in the Shinkansen bullet train gearbox where the temperature in the gear box is monitored and an SMA spring actuates a valve to adjust the oil level in the gearbox [116]. Other applications developed for trains include the thermally actuated switch for the radiator fan in diesel engines and steam traps for the steam heating system in passenger trains. Both of these applications utilize the shape memory effect.

1.10.4 Other Applications

In addition to the aerospace, transportation and medical industries, there are many other fields and applications that incorporate SMAs. The oil industry has shown extensive interest to use the SMA actuation capabilities in release devices and protection systems for downhole drilling equipment. The high operating conditions have also opened the avenue for the use of HTSMAs in these devices [117]. Everyday applications such as coffee makers and rice cookers have also incorporated SMAs. A rice cooker equipped with an SMA valve has the valve actuate when the cooker reaches a certain temperature and releases the excess steam in the chamber. SMA actuated louvers have also been incorporated in air conditioning vents that can adjust depending on the temperature of the air exiting the vents. The SME is also utilized in shower faucet designs where an SMA spring automatically adjusts the flow of hot and cold water to maintain a preset water temperature [118].

The pseudoelastic behavior has also been used in a wide range of applications. Developers of vibration control devices in civil structures have shown interest in pseudoelastic behavior of NiTi due to its capability to dissipate energy through a large hysteresis [119]. Other applications that employ the pseudoelastic behavior are flexible metallic eyeglasses and headphones, that

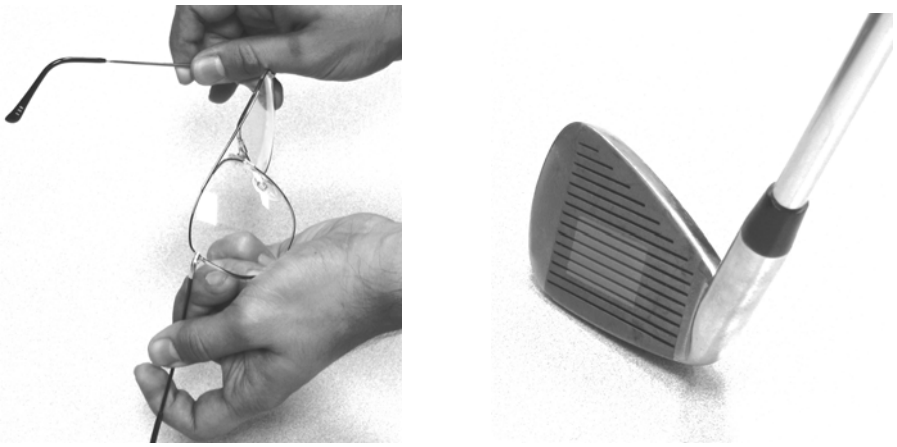

(a) (b)

Fig. 1.27. Commercial pseudoelastic applications of SMAs. **(a)** Pseudoelastic eye glass frames. **(b)** Golf club with embedded pseudoelastic SMA insert.

can be bent without breaking [77]. SMAs have also been used in sporting goods like golf clubs where the SMA embedded in the club absorbs the impact of the strike. Figure 1.27 shows a picture of a pseudoelastic eye glass frame and a golf club with a pseudoelastic SMA embedded in it.

In a recent study, an innovative approach of knitting SMA wires into different patterns has shown to produce complex shape changes such as rolling, spiraling, arching and folding [120]. The ability to generate such unique configurations using SMAs can open prospects for other novel design applications.

1.11 Summary

This chapter introduced the unique characteristic behaviors of shape memory alloys such as the shape memory effect and pseudoelasticity and discussed the underlying microstructural changes associated with such behaviors. The crystallography of martensitic transformation was also discussed, and a brief overview of the effects of alloying on the transformation behavior was presented. Some current implementation of SMAs into industrial and medical applications have also been discussed. As previously mentioned, several other compilations of work performed on SMAs are available. For historical work on SMAs the reader can refer to Perkins [3]. For application considerations, Duerig and coworkers provide a comprehensive summary. For details on microstructural influence on the behavior of SMAs, see Funakubo [4] and Otsuka and Wayman [5]. A more recent compilation of work by Brailovski and coworkers [121] gives an extensive summary on characterization efforts focused on SMAs.

1.12 Problems

1.1. Identify at least one biomedical application for which both the SME and the pseudoelastic effect could provide a solution.

1.2. A space application requires the use of an SMA component for fast actuation. The ambient temperature to which the SMA will be exposed is −30 °C. What properties would govern the choice of a suitable SMA? Suggest an alloy that would be most suited for such an application from the different alloys discussed in Sect. 1.9.

1.3. An SMA wire exhibits 5% recoverable strain upon mechanical unloading. When the wire is cooled, the material expands by 3% and recovers its shape upon heating. What are the different behaviors observed here?

1.4. An industrial process requires a small pressure vessel for storing hot gas. The pressure and the temperature inside the vessel cannot exceed 300 MPa and 80 °C, respectively. Suggest two concepts that implement SMAs in the design of a safety device for the pressure vessel. Suggest an SMA for this application making suitable arguments.

1.5. A particular actuation mechanism in an industry utilizes a temperature sensor that sends a signal to a motor which in turn operates a ratchet-pinion mechanism. The entire setup is fit into a small compartment. The company is searching for a suitable alternative actuation mechanism and is considering the use of SMAs. List the advantages of using SMAs in this particular application.

1.6. A particular application requires multiple cyclic actuation where the actuator needs to expand at high temperature and contract as the temperature decreases. The device assembly or the conditions of operation do not exert any stress on the actuator. How could one use an SMA for such an application?

1.7. A new pair of spectacle frames in the market has the capability to be twisted substantially without failure. Although the frame is made of an SMA, this flexible behavior is not due to a stress induced phase transformation phenomenon. Could this statement be true? Explain.

1.8. Shown in Fig. 1.28 is a simple heat engine. The SMA spring is actuated by resistive heating. A mass of 0.45 kg is suspended on the spring, which has an initial length of 3 cm. The current through and the voltage across the spring are 2 Amps and 6 Volts, respectively. When heated from T$< M_f$ to T$> A_f$, the tip of the spring moves from 12.5 cm (spring length under load) to 5 cm in 5 seconds. With the provided data answer the following questions:

1. What is the amount of work done by the spring?
2. What is the potential energy stored in the spring in the austenitic and martensitic states?

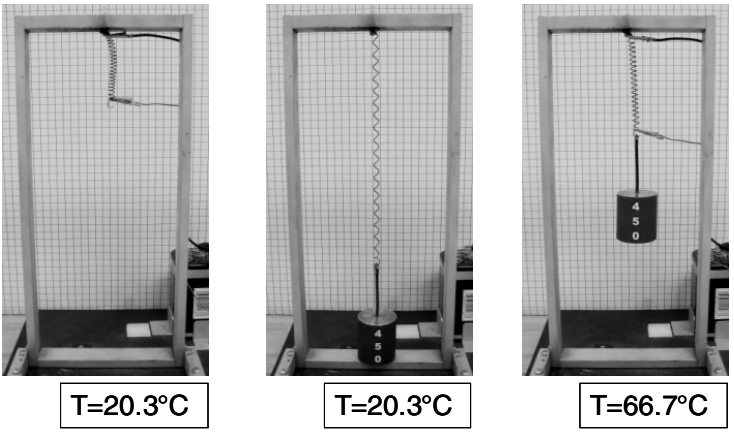

Fig. 1.28. The SMA heat engine.

3. What is the efficiency of the SMA spring?
4. Express the Carnot efficiency of an SMA heat engine, in terms of its transformation temperatures, assuming that the SMA heat engine operates at a nominal stress of 100 MPa, and that the transformation temperatures are shifted by 5 MPa/ °C in the presence of stress. From the SMAs presented in the chapter, select the ones with the highest Carnot efficiency.

1.9. Plot a schematic of the stress-strain response of an SMA specimen when it is thermomechanically loaded along loading paths 1 and 2, shown in the phase

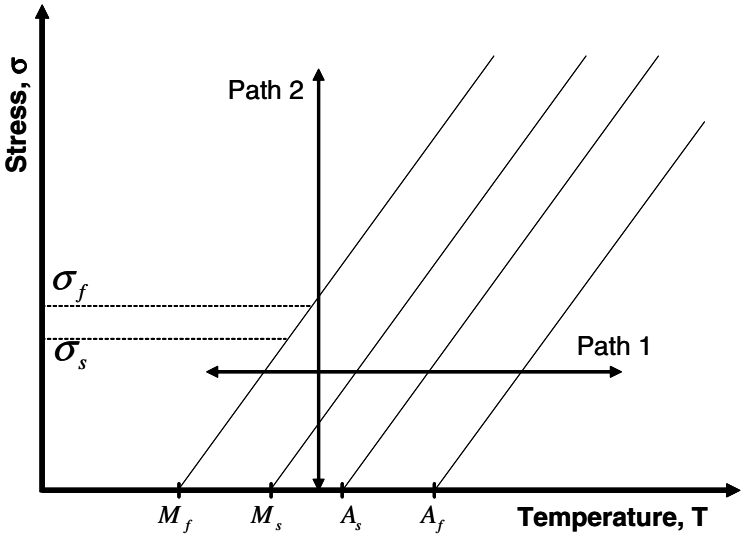

Fig. 1.29. Stress-temperature phase diagram.

diagram in Fig. 1.29. Note that the initial state of the material is austenitic for loading in path 2.

1.10. Compare the shape memory effect exhibited by shape memory alloys with the shape memory effect of shape memory polymers. In particular, compare the steps required to demonstrate the shape memory effect in two coils made of the two different shape memory materials.

1.11. The deployment of solar panels in spacecraft has been attempted by SMA strips (see Fig. 1.23), acting as temperature actuated hinges. Assuming that such hinges are provided in an initial flat shape, describe the process of shape setting for the hinges, so that they can deploy the solar panels upon heating.

References

[1] C. M. Jackson, H. J. Wagner, R. J. Wasilewski, 55-Nitinol—The alloy with a memory: Its physical metallurgy, properties and applications, Tech. Rep. NASA SP-5110, NASA Technology Utilization Office, Washington, D.C. (1972).
[2] T. Duerig, K. Melton, D. Stockel, C. Wayman (Eds.), Engineering Aspects of Shape Memory Alloys, Butterworth-Heinemann, London, 1990.
[3] J. Perkins, Shape Memory Effects in Alloys, Plenum Press, New York, 1975.
[4] H. Funakubo (Ed.), Shape Memory Alloys, Gordon and Breach Science Publishers, 1987.
[5] K. Otsuka, C. M. Wayman (Eds.), Shape Memory Materials, Cambridge University Press, Cambridge, 1999.
[6] G. V. Kurdjumov, L. G. Khandros, First reports of the thermoelastic behaviour of the martensitic phase of Au-Cd alloys, Doklady Akademii Nauk SSSR 66 (1949) 211–213.
[7] W. J. Buehler, J. V. Gilfrich, R. C. Wiley, Effects of low-temperature phase changes on the mechanical properties of alloys near composition TiNi, Journal of Applied Physics 34 (1963) 1475.
[8] F. E. Wang, W. J. Buehler, S. J. Pickart, Crystal structure and a unique "martensitic" transition of TiNi, Journal of Applied Physics 36 (3232-3239).
[9] L. Schetky, Shape-memory alloys, Scientific American 241 (74-82).
[10] M. Wayman, J. Harrison, The origins of the shape memory effect, Journal of Minerals, Metals, and Materials 41 (99) (1989) 26–28.
[11] M. H. Wu, L. M. Schetky, Industrial applications for shape memory alloys, in: Proceedings of the International Conference on Shape Memory and Superelastic Technologies, Pacific Grove, California, 2000.

[12] H. C. Doonkersloot, V. Vucht, Martensitic transformations in Au-Ti, Pd-Ti and Pt-Ti alloys, Journal of Less-Common Metals 20 (1970) 83–91.
[13] K. Melton, O. Mercier, Deformation behavior of NiTi-based alloys, Metallic Tras. 9A (1978) 1487–14488.
[14] S. Miyazaki, K. Mizukoshi, T. Ueki, T. Sakuma, Y. Liu, Fatigue life of Ti-50 at. Science and Engineering (1999) 658–663.
[15] K. Ullakko, J. K. Huang, C. Kantner, R. C. O'Handley, V. V. Kokorin, Large magnetic-field-induced strains in Ni_2MnGa single crystals, Applied Physics Letters 69 (13) (1996) 1966–1968.
[16] H. E. Karaca, I. Karaman, B. Basaran, Y. I. Chumlyakov, H. J. Maier, Magnetic field and stress induced martensite reorientation in NiMnGa ferromagnetic shape memory alloy single crystals, Acta Materialia 54 (1) (2006) 233–245.
[17] L. Contardo, G. Guenin, Training and two way memory effect in Cu-Zn-Al alloy, Acta Metallurgica 38 (7) (1990) 1267–1272.
[18] D. A. Miller, D. C. Lagoudas, Thermo-mechanical characterization of NiTiCu and NiTi SMA actuators: Influence of plastic strains, Smart Materials and Structures 9 (5) (2000) 640–652.
[19] X. Ren, K. Otsuka, Universal symmetry property of point defects in crystals, Physical Review Letters 85 (5) (2000) 1016–1019.
[20] P. Rodriguez, G. Guenin, Stability of the two way memory effect during thermal cycling of a high m_s temperature Cu-Al-Ni alloy, Materials Science Forum 56–58 (2) (1990) 541–546.
[21] D. A. Miller, D. C. Lagoudas, Influence of cold work and heat treatment on the shape memory effect and plastic strain development of NiTi, Material Science & Engineering A 308 (2001) 161–175.
[22] K. N. Melton, O. Mercier, Fatigue of NiTi thermoelastic martensites, Acta Metallurgica 27 (1979) 137–144.
[23] H. Tobushi, T. Hachisuka, S. Yamada, P. H. Lin, Rotating-bending fatigue of a TiNi shape-memory alloy wire, Mechanics of Materials 26 (1997) 35–42.
[24] J. L. McNichols, P. C. Brooks, NiTi fatigue behavior, Journal of Applied Physics 52 (1981) 7442–7444.
[25] H. Tobushi, T. Hachisuka, T. Hashimoto, S. Yamada, Cyclic deformation and fatigue of a TiNi shape memory alloy wire subjected to rotating bending, Journal of Engineering Materials and Technology 120 (1998) 64–70.
[26] D. Miller, Thermomechanical characterization of plastic deformation and transformation fatigue in shape memory alloys, Ph.D. thesis, Texas A&M University (2000).
[27] O. Bertacchini, D. Lagoudas, E. Patoor, Fatigue life characterization of shape memory alloys undergoing thermomechanical cyclic loading, Proceedings of SPIE, Smart Structures and Materials (2003) 612–624.

[28] K. Gall, H. Maier, Cyclic deformation mechanisms in precipitated NiTi shape memory alloys, Acta Materialia 50 (2002) 4643–4657.
[29] G. Eggeler, E. Hornbogen, A. Yawny, A. Heckmann, M. Wagner, Structural and functional fatigue of NiTi shape memory alloys, Materials Science and Engineering A (378) (2004) 24–33.
[30] W. Predki, M. Klönne, A. Knopik, Cyclic torsional loading of pseudoelastic NiTi shape memory alloys: Damping and fatigue failure, Materials Science and Engineering A (417) (2006) 182–189.
[31] K. Madangopal, The self accomodating martensitic microstructure of NiTi shape memory alloys, Acta Materialia 45 (12) (1997) 5347–5365.
[32] W. J. Buehler, R. C. Wiley, Nickel-base alloys, U.S. Patent 3,174,851. (1965).
[33] S. Miyazaki, K. Otsuka, Deformation and transformation behavior associated with the r-phase in Ti-Ni alloys., Metallurgical Transactions A 17A (1986) 53–63.
[34] D. Hartl, B. Volk, D. C. Lagoudas, F. T. Calkins, J. Mabe, Thermomechanical characterization and modeling of Ni60Ti40 SMA for actuated chevrons, in: Proceedings of ASME, International Mechanical Engineering Congress and Exposition (IMECE), 5–10 November, Chicago, IL, 2006, pp. 1–10.
[35] K. Richardson, Nitinol technologies innovator redefining the cutting edge, Outlook 22 (2) (2001) 1–8.
[36] D. J. Clingman, F. T. Calkins, J. P. Smith, Thermomechanical properties of 60-Nitinol, in: Proceedings of the SPIE, Smart Structures and Materials: Active Materials: Behavior and Mechanics, Vol. 5053, 2003, pp. 219–229.
[37] J. Mabe, R. Ruggeri, F. T. Calkins, Characterization of nickel-rich nitinol alloys for actuator development, in: Proceedings of the International Conference on Shape Memory and Superelasticity Technology, 2006.
[38] T. H. Nam, T. Saburi, K. Shimizu, Copper-content dependence of shape memory characteristics in Ti-Ni-Cu alloys, Materials Transactions, JIM 31 (11) (1990) 959–967.
[39] T. Saburi, T. Takagi, S. Nenno, K. Koshino, in: M. Doyama, S. Somlya, R. P. H. Chang (Eds.), Shape Memory Materials, MRS International Meeting on Advanced Materials, Vol. 9, 1989, pp. 147–152.
[40] N. M. Matveeva, V. N. Khachin, V. P. Shivokha, Stable and metastable phase equilibrium in metallic systems, Nauka, Moscow, 1985.
[41] Y. Liu, Mechanical and thermomechanical properties of a $Ti_{0.50}Ni_{0.25}Cu_{0.25}$ melt spun ribbon, Materials Science and Engineering A 354 (2003) 286–291.
[42] Z. L. Xie, J. Van Humbeeck, Y. Liu, L. Delaey, TEM study of Ti50Ni25Cu25 melt spun ribbons, Scripta Materialia 37 (3) (1997) 363–371.
[43] K. N. Melton, J. Simpson, T. W. Duerig, A new wide hysteresis NiTi based shape memory alloy and its applications, in: Proceedings of The

International Conference on Martensitic Transformations, The Japan Institute of Metals, 1986, pp. 1053–1058.

[44] K. N. Melton, J. L. Proft, T. W. Duerig, Wide hysteresis shape memory alloys based on the Ni -Ti -Nb system, MRS 9 (1989) 165–170.

[45] L. C. Zhao, T. W. Duerig, S. Justi, K. N. Melton, J. L. Proft, W. Yu, C. M. Wayman, The study of niobium-rich precipitates in a Ni-Ti-Nb shape memory alloy, Scripta Metallurgica and Materialia 24 (1990) 221–226.

[46] C. S. Zhang, L. C. Zhao, T. W. Duerig, C. M. Wayman, Effects of deformation on the transformation hysteresis and shape memory effect in a Ni47Ti44Nb9 alloy, Scripta Metallurgica and Materialia 2 (1990) 1807–1812.

[47] M. Piao, K. Otsuka, S. Miyazaki, H. Horikawa, Mechanism of the as temperature increase by pre-deformation in thermoelastic alloys, Materials Transactions, JIM 34 (10) (1993) 919–929.

[48] X. M. He, L. J. Rong, D. S. Yan, Y. Y. Li, TiNiNb wide hysteresis shape memory alloy with low niobium content, Materials Science and Engineering A 371 (2004) 193–197.

[49] P. G. Lidquist, C. M. Wayman, Shape memory and transformation behavior of martensitic Ti-Pd-Ni and Ti-Pt-Ni alloys, in: T. W. Duerig, K. N. Melton, D. Stöckel, C. M. Wayman (Eds.), Engineering Aspects of Shape Memory Alloys, Butterworth-Heinemann, London, 1990, pp. 58–68.

[50] P. E. Thoma, J. J. Boehm, Effect of composition on the amount of second phase and transformation temperatures of NixTi90-xHf10 shape memory alloys, Materials Science and Engineering A 273-275 (1999) 385–389.

[51] V. N. Khachin, N. A. Matveeva, V. P. Sivokha, D. V. Chernov, High-temperature shape memory effects in TiNi-TiPd system alloys, Doklady Akademii Nauk SSSR (USSR) 257 (1) (1981) 167–169.

[52] S. Wu, C. Wayman, Martensitic transformations and the shape-memory effect in $Ti_{50}Ni_{10}Au_{40}$ and $Ti_{50}Au_{50}$ alloys, Metallography (1987) 359.

[53] P. K. Kumar, D. C. Lagoudas, K. J. Zanca, M. Z. Lagoudas, Thermomechanical characterization of high temperature SMA actuators, in: Proceedings of SPIE, Vol. 6170, 2006, pp. 306–312.

[54] S. Padula II, G. Bigelow, R. Noebe, D. Gaydosh, A. Garg, Challenges and progress in the development of high-temperature shape memory alloys based on NiTiX compositions for high-force actuator applications, in: Proceedings of the International Conference on Shape Memory and Superelastic Technologies, ASM International, Metals Park, OH, 2006.

[55] Z. Pu, H. Tseng, K. Wu, Martensite transformation and shape-memory effect of NiTi-Zr high- temperature shape-memory alloys, in: SPIE proceedings, Vol. 2441, 1995, p. 171.

[56] B. Strnadel, S. Ohashi, H. Ohtsuka, T. Ishihara, S. Miyazaki, Cyclic stress-strain characteristics of Ti-Ni and Ti-Ni-Cu shape memory alloys, Material Science & Engineering A 202 (1995) 148–156.

[57] P. Potapov, A. Shelyakov, A. Gulyaev, E. Svistunova, N. Matveeva, D. Hodgson, Effect of hf on the structure of Ni-Ti martensitic alloys, Materials Letters 32 (4) (1997) 247–250.

[58] S. Hsieh, S. Wu, Room-temperature phases observed in $Ti_{53-x}Ni_{47}Zr_x$ high-temperature shape memory alloys, Journal of Alloys and Compounds 226 (1998) 276–282.

[59] K. Enami, S. Menno, Metal transformation 2 (1971).

[60] R. Kainuma, M. Ise, C. Jia, H. Ohtani, K. Ishida, Phase equilibria and microstructural control in the Ni-Co-Al system, Intermetallics 4 (1996) 151.

[61] D. Schryvers, P. Boullay, P. Potapov, R. Kohn, J. Ball, Microstructures and interfaces in Ni-Al martensite: comparing HRTEM observations with continuum theories, International Journal of Solids Structures 39 (3543).

[62] H. E. Karaca, I. Karaman, D. C. Lagoudas, H. J. Maier, Y. I. Chumlyakov, Recoverable stress-induced martensitic transformation in a ferromagnetic CoNiAl alloy, Scripta Materialia 49 (2003) 831–836.

[63] H. Morito, A. Fujita, R. Kainuma, K. Ishida, K. Oikawa, Magnetocrystalline anisotropy in single-crystal Co-Ni-Al ferromagnetic shape-memory alloy, Applied Physics Letters 81 (9) (2002) 1657–1659.

[64] P. J. Webster, K. R. A. Ziebeck, S. L. Town, M. S. Peak, Magnetic order and phase transformation in Ni_2MnGa, Philosophical Magazine B 49 (3) (1984) 295–310.

[65] S. J. Murray, M. Marioni, S. M. Allen, R. C. O'Handley, 6% magnetic-field-induced strain by twin-boundary motion in ferromagnetic Ni-Mn-Ga, Applied Physics Letters 77 (6) (2000) 886–888.

[66] R. C. O'Handley, S. M. Allen, D. I. Paul, C. P. Henry, M. Marioni, D. Bono, C. Jenkins, A. Banful, R. Wager, Keynote address: Magnetic field-induced strain in single crystal Ni-Mn-Ga, Proceedings of SPIE, Symposium on Smart Structures and Materials 5053 (2003) 200–206.

[67] A. Sozinov, A. A. Likhachev, N. Lanska, O. Söderberg, K. Ullakko, V. K. Lindroos, Effect of crystal structure on magnetic-field-induced strain in Ni-Mn-Ga, Proceedings of SPIE, Symposium on Smart Structures and Materials 5053 (2003) 586–594.

[68] H. Karaca, I. Karaman, B. Basaran, D. Lagoudas, Y. Chumlyakov, H. Maier, On the stress-assisted magnetic-field-induced phase transformation in ni_2mnga ferromagnetic shape memory alloys, Acta Materialia 55 (2007) 4253–4269.

[69] J. Cui, T. W. Shield, R. D. James, Phase transformation and magnetic anisotropy of an iron-palladium ferromagnetic shape-memory alloy, Acta Materialia 52 (2004) 35–47.

[70] R. D. James, M. Wuttig, Magnetostriction of martensite, Philosophical Magazine A 77 (5) (1998) 1273–1299.
[71] T. W. Shield, Magnetomechanical testing machine for ferromagnetic shape-memory alloys, Review of Scientific Instruments 74 (9) (2003) 4077–4088.
[72] T. Yamamoto, M. Taya, Y. Sutou, Y. Liang, T. Wada, L. Sorensen, Magnetic field-induced reversible variant rearrangement in Fe-Pd single crystals, Acta Materialia 52 (17) (2004) 5083–5091.
[73] S. J. Murray, R. Hayashi, M. Marioni, S. M. Allen, R. C. O'Handley, Magnetic and mechanical properties of FeNiCoTi and NiMnGa magnetic shape memory alloys, Proceedings of SPIE 3675 (1999) 204–211.
[74] A. Fujita, K. Fukamichi, F. Gejima, R. Kainuma, K. Ishida, Magnetic properties and large magnetic-field-induced strains in off-stoichiometric Ni-Mn-Al heusler alloys, Applied Physics Letters 77 (19) (2000) 3054–3056.
[75] M. Wuttig, J. Li, C. Craciunescu, A new ferromagnetic shape memory alloy system, Scripta Materialia 44 (2001) 2393–2397.
[76] T. Sakamoto, T. Fukuda, T. Kakeshita, T. Takeuchi, K. Kishio, Magnetic field-induced strain in iron-based ferromagnetic shape memory alloys, Journal of Applied Physics 93 (10) (2003) 8647–8649.
[77] K. R. Melton, General applications of shape memory alloys and smart materials, in: K. Otsuka, C. M. Wayman (Eds.), Shape Memory Materials, Cambridge University Press, Cambridge, 1999, Ch. 10, pp. 220–239.
[78] C. Liang, F. Davidson, L. M. Schetky, F. K. Straub, Applications of torsional shape memory alloys actuators for active rotor blade control — opportunities and limitations, in: Proceedings of SPIE, Smart Structures and Materials: Smart Structures and Integrated Systems, Vol. 2717, 1996, pp. 91–100.
[79] L. J. Garner, L. N. Wilson, D. C. Lagoudas, O. K. Rediniotis, Development of a shape memory alloy actuated biomimetic vehicle, Smart Materials and Structures 9 (2000) 673–683.
[80] A. A. Ilyin, P. G. Sysolyatin, V. E. Gunter, A. P. Dergilev, M. A. Didin, S. P. Sysolyatin, I. A. Makarova, The use of superelastic shape memory implants in temporo-mandibular joint surgery, Proceedings of the First International Symposium on Advanced Biomaterials (ISAB), Montreal, Canada (1997) 177.
[81] V. Brailovski, F. Trochu, Review of shape memory alloys medical applications in Russia, Bio-Medical Materials & Engineering 6 (4) (1996) 291–298.
[82] B. Sanders, R. Crowe, E. Garcia, Defense advanced research projects agency – Smart materials and structures demonstration program overview, Journal of Intelligent Material Systems and Structures 15 (2004) 227–233.
[83] J. Kudva, Overview of the DARPA smart wing project, Journal of Intelligent Material Systems and Structures 15 (2004) 261–267.

[84] J. K. Strelec, D. C. Lagoudas, M. A. Khan, J. Yen, Design and implementation of a shape memory alloy actuated reconfigurable wing, Journal of Intelligent Material Systems and Structures 14 (2003) 257–273.
[85] R. Mani, D. Lagoudas, O. Rediniotis, MEMS based active skin for turbulent drag reduction, in: Proceedings of SPIE, Smart Structures and Materials, Vol. 5056, San Diego, CA, 2003, pp. 9–20.
[86] M. Tawfik, J. Ro, C. Mei, Thermal post-buckling and aeroelastic behaviour of shape memory alloy reinforced plates, Smart Materials and Structures 11 (2002) 297–307.
[87] C. Nam, A. Chattopadhyay, Y. Kim, Application of shape memory alloy (SMA) spars for aircraft maneuver enhancement, in: Proceedings of SPIE, Smart Structures and Materials, Vol. 4701, San Diego, CA, 2002, pp. 226–236.
[88] D. Pitt, J. Dunne, E. White, E. Garcia, SAMPSON smart inlet SMA powered adaptive lip design and static test, Proceedings of the 42nd AIAA Structures, Structrual Dynamics, and Materials Conference, Seattle, WA, 16–20 April 2001 (2001) 1–11.
[89] S. Wax, G. Fischer, R. Sands, The past, present, and future of DARPAs investment strategy in smart materials, Journal of the Minerals, Metals, and Materials Society 55 (12) (2003) 17–23.
[90] J. Mabe, R. Cabell, G. Butler, Design and control of a morphing chevron for takeoff and cruise noise reduction, in: Proceedings of the 26th Annual AIAA Aeroacoustics Conference, Monterey, CA, 2005, pp. 1–15.
[91] T. Turner, R. Buehrle, R. Cano, G. Fleming, Modeling, fabrication, and testing of a SMA hybrid composite jet engine chevron concept, Journal of Intelligent Material Systems and Structures 17 (2006) 483–497.
[92] J. H. Mabe, F. Calkins, G. Butler, Boeing's variable geometry chevron, morphing aerostructure for jet noise reduction, in: 47th AIAA/ ASME / ASCE / AHS / ASC Structures, Structural Dynamics and Materials Conference, Newport, Rhode Island, 2006, pp. 1–19.
[93] V. Birman, Review of mechanics of shape memory alloy structures, Applied Mechanics Reviews 50 (11) (1997) 629–645.
[94] H. Prahlad, I. Chopra, Design of a variable twist tiltrotor blade using shape memmory alloy (SMA) actuators, in: Proceedings of SPIE, Smart Structures and Materials, Vol. 4327, Newport Beach, CA, 2001, pp. 46–59.
[95] A. Jacot, R. Ruggeri, D. Clingman, Shape memory alloy device and control method, U.S. Patent 7,037,076 (2 May 2006).
[96] K. Singh, J. Sirohi, I. Chopra, An improved shape memory alloy actuator for rotor blade tracking, Journal of Intelligent Material Systems and Structures 14 (2003) 767–786.
[97] D. Kennedy, F. Straub, L. Schetky, Z. Chaudhry, R. Roznoy, Development of an SMA actuator for in-flight rotor blade tracking, Journal of Intelligent Material Systems and Structures 15 (2004) 235–248.

[98] R. Loewy, Recent developments in smart structures with aeronautical applications, Smart Materials and Structures 6 (1997) R11–R42.
[99] C. Test, S. Leone, S. Ameduri, A. Concilio, Feasibility study on rotorcraft blade morphing in hovering, in: Proceedings of SPIE, Smart Structures and Materials, Vol. 5764, San Diego, CA, 2005, pp. 171–182.
[100] A. Johnson, Non-explosive seperation device, U.S. Patent 5,119,555 (June 1992).
[101] O. Godard, M. Lagoudas, D. Lagoudas, Design of space systems using shape memory alloys, in: Proceedings of SPIE, Smart Structures and Materials, Vol. 5056, San Diego, CA, 2003, pp. 545–558.
[102] C. Willey, B. Huettl, S. Hill, Design and development of a miniature mechanisms tool-kit for micro spacecraft, in: Proceedings of the 35th Aerospace Mechanisms Symposium, Ames Research Center, 9–11 May, 2001, pp. 1–14.
[103] A. Peffer, K. Denoyer, E. Fossness, D. Sciulli, Development and transition of low-shock spacecraft release devices, in: Proceedings of IEEE Aerospace Conference, Vol. 4, 2000, pp. 277–284.
[104] B. Carpenter, J. Lyons, EO-1 technology validation report: Lightweight flexible solar array experiment, Tech. rep., NASA Godard Space Flight Center, Greenbelt, MD (8 August 2001).
[105] S. Shabalovskaya, Biological aspects of TiNi alloys surfaces, Journal de Physique IV 5 (1995) 1199–1204.
[106] J. Ryhänen, Biocompatibility evolution of nickel-titanium shape memory alloy, Ph.D. thesis, Univeristy of Oulu, Oulu, Finland (1999).
[107] L. Machado, M. Savi, Medical applications of shape memory alloys, Brazilian Journal of Medical and Biological Research 36 (2003) 683–691.
[108] D. Mantovani, Shape memory alloys: Properties and biomedical applications, Journal of the Minerals, Metals and Materials Society 52 (2000) 36–44.
[109] K. Speck, A. Fraker, Anodic polarization behavior of Ti-Ni and Ti-6Al-4V in simulated physiological solutions, J Dent Res 59 (100) (1980) 1590–1595.
[110] G. Andreasen, T. Hilleman, An evaluation of 55 cobalt subsituted nitinol wire for use in orthodontics, Journal of the American Dental Association 82 (1971) 1373–1375.
[111] S. Thompson, An overview of nickel-titanium alloys used in dentistry, International Endodontic Journal 33 (2000) 297–310.
[112] T. Duerig, A. Pelton, D. Stöckel, Superelastic nitinol for medical devices, Medical Plastics and Biomaterials (1997) 31–42.
[113] D. Lagoudas, E. Vandygriff, Processing and characterization of niti porous sma by elevated pressure sintering, Journal of intelligent material system and structures 13 (2002) 837–850.

[114] J. Paine, C. Rogers, High velocity impact response of composites with surface bonded nitinol-SMA hybrid layers, Journal of Intelligent Material Systems and Structures 5 (4) (1994) 530–535.
[115] B. Barnes, D. B. J. Luntz, A. Browne, K. Strom, Panel deployment using ultrafast SMA latches, in: ASME International Mechanical Engineering Congress and Exposition, Chicago, Illinois, USA, 2006.
[116] K. Otsuka, T. Kakeshita, Science and technology of shape-memory alloys: New developments, bulletin (February 2002).
[117] P. Anderson, A., S. Sangesland, Detailed study of shape memory alloys in oil well applications., Sintef petroleum research, Trondheim, Norway (1999).
[118] I. Ohkata, Y. Suzuki, The design of shape memory alloy actuators and their applications, in: K. Otsuka, C. M. Wayman (Eds.), Shape Memory Materials, Cambridge University Press, Cambridge, 1999, Ch. 11, pp. 240–266.
[119] S. Saadat, J. Salichs, M. Noori, Z. Hou, H. Davoodi, I. Bar-on, An overview of vibration and seismic applications of NiTi shape memory alloy, Smart Materials and Structures 11 (2002) 218–229.
[120] J. Evans, D. Brei, J. Luntz, Preliminary experimental study of SMA knitted actuation architectures, in: ASME International Mechanical Engineering Congress and Exposition, 2006.
[121] V. Brailovski, S. Prokoshkin, P. Terriault, F. Trochu (Eds.), Shape Memory Alloys: Fundamentals, Modeling and Applications, University of Quebec, 2003.